Delft University of Technology

Quadrotor Fault Tolerant Incremental Sliding Mode Control driven by Sliding Mode Disturbance Observers

Wang, Xuerui; Sun, Sihao; van Kampen, Erik Jan; Chu, Qiping

Important note
To cite this publication, please use the final published version (if applicable).
Please check the document version above.

Quadrotor Fault Tolerant Incremental Sliding Mode Control driven by Sliding Mode Disturbance Observers

Xuerui Wang *, Sihao Sun, Erik-Jan van Kampen, Qiping Chu

Delft University of Technology, Kluyverweg 1, 2629HS Delft, the Netherlands

A B S T R A C T

This paper proposes an Incremental Sliding Mode Control driven by Sliding Mode Disturbance Observers (INDI-SMC/SMDO), with application to a quadrotor fault tolerant control problem. By designing the SMC/SMDO based on the control structure of the sensor-based Incremental Nonlinear Dynamic Inversion (INDI), instead of the model-based Nonlinear Dynamic Inversion (NDI) in the literature, the model dependency of the controller and the uncertainties in the closed-loop system are simultaneously reduced. This allows INDI-SMC/SMDO to passively resist a wider variety of faults and external disturbances using continuous control inputs with lower control and observer gains. When applied to a quadrotor, both numerical simulations and real-world flight tests demonstrate that INDI based SMC/SMDO has better performance and robustness over NDI based SMC/SMDO, in the presence of model uncertainties, wind disturbances, and sudden actuator faults. Moreover, the implementation process is simplified because of the reduced model dependency and smaller uncertainty variations of INDI-SMC/SMDO. Therefore, the proposed control method can be easily implemented to improve the performance and survivability of quadrotors in real life.

© 2019 Elsevier Masson SAS. All rights reserved.

1. Introduction

Characterized by mechanical simplicity, high maneuverability, and task adaptability, autonomous quadrotors have attracted considerable interests in academic and industrial communities. A recent research revealed the usage of quadrotors has a potential for reducing the greenhouse gas emissions and energy consumption [1]. Due to the lack of redundancies, rotor failures have high impacts on quadrotor safety. To make widespread applications of quadrotors possible in the future, improving their reliability while maintaining affordability becomes more and more important.

Being invariant (better than just robust) to matched uncertainties [2,3], Sliding Mode Control (SMC) is a promising candidate to fulfill this goal. A variety of SMC methods have been proposed for quadrotors to resist external disturbances and to cope with faults [4–14]. In spite of the varieties in SMC designs, for most SMC algorithms, the required control gains are positively correlated with uncertainty bounds (for first-order SMC), or the bounds of uncertainty derivatives (for higher-order SMC). However, high-gain SMC methods are problematic, they amplify the measurement noise, excite unmodeled dynamics, and aggravate the well-known

chattering phenomenon [15]. On account of these side-effects, one of the research focuses in the SMC community is on achieving the minimum possible value of the SMC gains [15–18].

Two effective approaches can be used to reduce the SMC gains. One is using a continuous model-based preliminary feedback control term to roughly cancel the nonlinearities and dynamic couplings, such that only the remaining uncertainties need to be compensated by SMC. Regrading nonlinear control problems, this feedback term is commonly derived by dynamically inverting nonlinear algebraic equations, namely, by using Nonlinear Dynamic Inversion (NDI). Examples can be given for both first-order [4–9,12, 19] and higher-order [11,13,20,21] sliding mode control methods. The other approach is incorporating the uncertainty estimations, for example by using Sliding Mode Disturbance Observers (SMDO), such that only the estimation errors need to be dealt with by SMC [8,13,19,22]. Although these two approaches have their advantages, it is impractical and tedious to pursue a perfect model. Moreover, the switching gains used in SMDO still need to be larger than the uncertainty bounds or their derivatives [8,13,19,22]. Even though continuity can be retained by using a filtering process in the equivalent control estimations of SMDO, the high-frequency switching component can only be attenuated instead of being totally rejected [19]. Therefore, it is valuable to design a control method which could fundamentally reduce the control efforts of SMC/SMDO whilst requiring less model knowledge.

Incremental Nonlinear Dynamic Inversion (INDI) is a sensor-based control method, which not only has less model dependency, but also obtains better robustness as compared to the NDI control [23,24]. INDI was initially proposed in [25], and has been successfully applied on the angular rate control [26] and position control [27] problems of quadrotors. Flight tests on a CS-25 certified passenger aircraft demonstrate that INDI outperforms NDI, in the presence of model uncertainties, sensor noises, and real-world disturbances [23]. Recently, this INDI control method was reformulated in [24] to broaden its applicability. The stability and robustness of this method are also analyzed in [24] using Lyapunov methods and the nonlinear system perturbation theories. It has been proved in [24] that for a nonlinear system with stable internal dynamics, if the remaining regular perturbation term in INDI is bounded, then the states will be ultimately bounded by a class $\mathcal{K}$ function of the regular perturbation bound. Although the ultimate bound of the states can be reduced by increasing the sampling frequency and the control gains, these two approaches have practical limitations.

A nonlinear control framework named Incremental Sliding Mode Control (INDI-SMC), which hybridizes the reformulated INDI with SMC was proposed in [28]. This hybridization inherits the advantages and remedies the drawbacks of both methods. On the one hand, by introducing a SMC term into INDI, the influences of the remaining regular perturbation term can be compensated. On the other hand, by designing SMC based on the sensor-based INDI control framework, the model dependency and the minimum possible control gains of SMC can simultaneously be reduced. Nevertheless, Ref. [28] still has some limitations. First of all, the influences of sudden faults were not explicitly considered in the control derivations and the stability analyses. Also, the external disturbances were not included in the control derivations, analyses and simulation tests. Finally, only a classical first-order SMC hybridized with INDI was numerically verified in [28], whilst the consequences of incorporating SMDO have not been demonstrated yet. These issues will be dealt with in the present paper.

The main contributions of this paper are the proposal of Incremental Sliding Model Control driven by Sliding Mode Disturbance Observers (INDI-SMC/SMDO), and its application to a quadrotor fault tolerant control problem. Apart from its lower model dependency, the proposed method also has improved robustness and performance as compared to SMC/SMDO designs based on NDI in the literature. Moreover, by virtue of the sensor-based characteristic of INDI, the control objectives can be achieved using lower switching gains, which effectively mitigates the chattering effects of SMC. Furthermore, a wider range of disturbances and faults can be passively resisted without gain adaption. Finally, the effectiveness of this method is verified by both numerical simulations and real-world flight tests.

The structure of this paper is as follows: Sec. 2 proposes the INDI-SMC/SMDO method and analyzes its stability and robustness. Theoretical comparisons with NDI based SMC/SMDO are also conducted in Sec. 2. Both the NDI and INDI based SMC/SMDO methods are applied to a quadrotor fault tolerant control problem in Sec. 3. The effectiveness of the proposed INDI-SMC/SMDO method is demonstrated by simulations in Sec. 4 and by flight tests in Sec. 5. Main conclusions are drawn in Sec. 6.

2. Incremental sliding mode control driven by sliding mode disturbance observers

Consider a nonlinear multi-input/multi-output control-affine system:

$$\dot{\boldsymbol{x}} = \boldsymbol{f}(\boldsymbol{x}, \kappa(t)) + \boldsymbol{G}(\boldsymbol{x}, \kappa(t))\boldsymbol{u} + \boldsymbol{d}(t), \quad \boldsymbol{y} = \boldsymbol{x} \tag{1}$$

where $\boldsymbol{x} \in \mathcal{R}^n$, $\boldsymbol{u} \in \mathcal{R}^n$, $\boldsymbol{f}(\boldsymbol{x}, \kappa(t)) \in \mathcal{R}^n$, $\boldsymbol{G}(\boldsymbol{x}, \kappa(t)) = [\boldsymbol{g}_1, \boldsymbol{g}_2, .., \boldsymbol{g}_n]$ $\in \mathcal{R}^{n \times n}$, $\boldsymbol{g}_i \in \mathcal{R}^n$, $i = 1, 2, ..., n$. $\boldsymbol{d} \in \mathcal{R}^n$ represents the bounded external disturbances. To indicate the sudden fault at $t = t_f$ during flight, $\kappa(t) \in \mathcal{R}$ is designed as a step function, with $t < t_f$, $\kappa = 0$ indicates the fault-free case and $t \geq t_f$, $\kappa = 1$ denotes the post-fault condition. $\boldsymbol{f}$ and $\boldsymbol{G}$ are expanded as:

$$\boldsymbol{f} = \bar{\boldsymbol{f}} + (\boldsymbol{f}_f - \bar{\boldsymbol{f}})\kappa + \hat{\boldsymbol{f}}, \quad \boldsymbol{G} = \bar{\boldsymbol{G}} + (\boldsymbol{G}_f - \bar{\boldsymbol{G}})\kappa + \hat{\boldsymbol{G}} \tag{2}$$

where $\bar{\boldsymbol{f}}$, $\bar{\boldsymbol{G}}$ are the nominal dynamics used for controller design, $\boldsymbol{f}_f$, $\boldsymbol{G}_f$ denote the post-fault dynamics, and $\hat{\boldsymbol{f}}$, $\hat{\boldsymbol{G}}$ represent the model uncertainties as continuous functions of $\boldsymbol{x}$.

Assumption 1. $\boldsymbol{G}(\boldsymbol{x}, \kappa(t))$ in Eq. (1) is nonsingular for all t.

Assumption 1 constrains the damage intensity considered in the present paper. If $\boldsymbol{G}(\boldsymbol{x}, \kappa(t))$ becomes singular because of faults, subspace control strategies need to be used. For example, a subspace control strategy is used in conjunction with Incremental Nonlinear Dynamic Inversion (INDI) in [29] for achieving the high speed flight (over 9 m/s) of a damaged quadrotor with complete loss of a single rotor.

The control aim is to design a continuous Sliding Mode Control (SMC) input that achieves decoupled asymptotic output tracking $\boldsymbol{y}_c - \boldsymbol{y} = \boldsymbol{e} \to \boldsymbol{0}$, in the presence of model uncertainties, external disturbances, and sudden faults. The output reference $\boldsymbol{y}_c$ should be differentiable with continuous $\dot{\boldsymbol{y}}_c$. In the context of the sliding mode control, the sliding variable $\boldsymbol{\sigma}$ is designed such that when $\boldsymbol{\sigma} = \boldsymbol{0}$ is reached, the desired error dynamics are achieved. For fair comparisons, a sliding variable designed as

$$\boldsymbol{\sigma} = \boldsymbol{e} + \boldsymbol{K}_c \int \boldsymbol{e} \mathrm{d}t \tag{3}$$

will be consistently used in this paper. $\boldsymbol{K}_c = \mathrm{diag}\{K_{c_i}\}$, $i = 1, 2, .., n$, and K_{c_i} are chosen to achieve desired error dynamics.

In subsection 2.1, SMC/Sliding Mode Disturbance Observer (SMDO) based on the control structure of NDI will be introduced first as a benchmark, then INDI-SMC/SMDO will be proposed in subsection 2.2. These two control approaches will be compared analytically in subsection 2.3.

2.1. NDI-SMC/SMDO

Using Eq. (1), the dynamics of the sliding variable in Eq. (3) are given by:

$$\dot{\boldsymbol{\sigma}} = \dot{\boldsymbol{e}} + \boldsymbol{K}_c \boldsymbol{e} = (\dot{\boldsymbol{y}}_c + \boldsymbol{K}_c \boldsymbol{e} - \bar{\boldsymbol{f}}) + (\bar{\boldsymbol{f}} - \boldsymbol{f} - \boldsymbol{d}) - \bar{\boldsymbol{G}}\boldsymbol{u} - (\boldsymbol{G} - \bar{\boldsymbol{G}})\boldsymbol{u}$$
$$\triangleq \bar{\boldsymbol{\Psi}} + \Delta\boldsymbol{\Psi} - \bar{\boldsymbol{G}}\boldsymbol{u} - \Delta\boldsymbol{G}\boldsymbol{u} \tag{4}$$

in which $\Delta\boldsymbol{\Psi}$ and $\Delta\boldsymbol{G}$ are unavailable for controller design. It is noteworthy that $\Delta\boldsymbol{G}$ represents the multiplicative uncertainties in the control effectiveness matrix, which was not considered in Ref. [8,19].

In order to reduce the control gains, SMC can be used along with SMDO, which can estimate bounded uncertainties. SMDO designs are independent of the model structure, only the bounds of uncertainties are needed by the classical SMDO designs, and the bounds of the uncertainty derivatives are required by the higher-order SMDO (e.g. Super-twisting SMDO [8,19,22]) designs. This paper designs a classical SMDO as an example, where the auxiliary sliding variables are introduced as:

$$\boldsymbol{s} = \boldsymbol{\sigma} + \boldsymbol{z}, \quad \dot{\boldsymbol{z}} = -\bar{\boldsymbol{\Psi}} + \bar{\boldsymbol{G}}\boldsymbol{u} - \boldsymbol{v}_0 \tag{5}$$

Substituting Eq. (4) into Eq. (5) yields:

$$\dot{s} = (\Delta\Psi - \Delta G u) - v_o \triangleq -\varepsilon_{\text{ndi}} - v_o \tag{6}$$

Denote the control input as u_{ndi}, then using Eqs. (2, 4), ε_{ndi} in Eq. (6) is rewritten as:

$$\begin{aligned}\varepsilon_{\text{ndi}} &= -\Delta\Psi + \Delta G u_{\text{ndi}}\\ &= [\hat{f} + \hat{G}u_{\text{ndi}} + d] + \kappa[(f_f - \bar{f}) + (G_f - \bar{G})u_{\text{ndi}}]\end{aligned} \tag{7}$$

Assumption 2. For all $x \in \mathcal{R}^n$, $\kappa \in \mathcal{R}$, and bounded external disturbance $d \in \mathcal{R}^n$, ε_{ndi} in Eq. (7) is bounded.

The boundedness of the perturbations is the precondition of many robust control methods. For example, Assumption 2 is made in [19,30–33]. Design v_o as:

$$v_o = K_s \text{Sign}(s) = [K_{s,1}\text{sign}(s_1), K_{s,2}\text{sign}(s_2), ..., K_{s,n}\text{sign}(s_n)]^T,$$
$$K_{s,i} \geq \eta + |\varepsilon_{\text{ndi},i}| \tag{8}$$

where η is a small positive constant. Then s is stabilized at zero in finite time. This can be proved by introducing a candidate Lyapunov function $V_1 = \frac{1}{2}s^T s$. Using Eqs. (6, 8), the time derivative of V_1 is:

$$\dot{V}_1 = s^T\dot{s} = s^T(-\varepsilon_{\text{ndi}} - v_o) \leq \sum_{i=1}^{n}|s_i||\varepsilon_{\text{ndi},i}| - K_{s,i}|s_i| \leq -\eta\sum_{i=1}^{n}|s_i| \tag{9}$$

$s^T\dot{s} \leq -\eta\sum_{i=1}^{n}|s_i|$ is referred to as the η reaching law, which ensures $s_i = 0$ is reached in finite time $t_{r,i} \leq |s_i(0)|/\eta$ [19,18]. Therefore, in view of Eq. (6), the equivalent control [2,19] $v_{\text{eq},i}$ estimates exactly $-\varepsilon_{\text{ndi},i}$, $\forall t_i \geq t_{r,i}$. One way to obtain v_{eq} is filtering v_o as $\hat{v}_{\text{eq},i}(s) = G_{LPF}(s)v_{o,i}(s)$, in which s is a Laplace variable and $G_{LPF}(s)$ is the transfer function of a low-pass filter. When first-order low-pass filters with time constant τ_i are used, $\hat{v}_{\text{eq}}$ estimates $-\varepsilon_{\text{ndi}}$ with a small estimation error proportional to τ_i, i.e. $|-\varepsilon_{\text{ndi},i} - \hat{v}_{\text{eq},i}| < \mathcal{O}(\tau_i)$. Using $\|\cdot\|$ to denote the 2-norm of a vector, then $\|\varepsilon_{\text{ndi}} + \hat{v}_{\text{eq}}\| < \mathcal{O}(\tau) \triangleq \|[\mathcal{O}(\tau_1), ..., \mathcal{O}(\tau_n)]^T\|$. As presented in [19], τ_i can be taken very small, and its lower boundary is the sampling interval of the onboard computer.

Following the SMDO design, the continuous SMC/SMDO control input that asymptotically stabilizes σ is designed as:

$$u_{\text{ndi}} = \bar{G}^{-1}(\bar{\Psi} + K_\sigma\sigma + \hat{v}_{\text{eq}}) \tag{10}$$

where $K_\sigma = \text{diag}\{K_{\sigma,i}\}$, $K_{\sigma,i} > 0$. Substituting Eqs. (6, 10) into Eq. (4) leads to $\dot{\sigma} = -K_\sigma\sigma + [\Delta\Psi - \Delta G u_{\text{ndi}}] - \hat{v}_{\text{eq}} = -K_\sigma\sigma - (\varepsilon_{\text{ndi}} + \hat{v}_{\text{eq}})$. Introduce a candidate Lyapunov function $V_2 = \sigma^T P\sigma$, where $P = P^T > 0$ is the solution of the Lyapunov equation $PK_\sigma + K_\sigma^T P = I$. $I \in \mathcal{R}^{n\times n}$ is an identity matrix. Then when $t > \max\{t_{r,i}\}$, the time derivative of V_2 is:

$$\begin{aligned}\dot{V}_2 &= -\sigma^T[PK_\sigma + K_\sigma^T P]\sigma - 2\sigma^T P(\varepsilon_{\text{ndi}} + \hat{v}_{\text{eq}})\\ &< -\|\sigma\|^2 + 2\|\sigma\|\|P\|\mathcal{O}(\tau)\\ &\leq -\gamma\|\sigma\|^2, \quad \forall\|\sigma\| \geq \frac{2\|P\|\mathcal{O}(\tau)}{1-\gamma}\end{aligned} \tag{11}$$

with constant $\gamma \in (0, 1)$. Eq. (11) proves that under Assumptions 1 and 2, the NDI-SMC/SMDO control law given by Eq. (10), in which $\hat{v}_{\text{eq}}$ is observed using a SMDO with gain condition given in Eq. (8), ensures that the state σ is ultimately bounded by a class $\mathcal{K}$ function [24,34] of $\mathcal{O}(\tau)$. Theoretically, this ultimate bound can be made arbitrarily small [19,31] by reducing τ_i and increasing $K_{\sigma,i}$.

Remark 1. The control input given by Eq. (10) is essentially based on the control structure of Nonlinear Dynamic Inversion (NDI), whose virtual control now contains three parts: the classical NDI virtual control $\dot{y}_c + K_c e$, the SMC virtual control $K_\sigma\sigma$, and the SMDO virtual control $\hat{v}_{\text{eq}}$. Therefore, Eq. (10) is referred to as NDI based SMC driven by SMDO in this paper, which is abbreviated to NDI-SMC/SMDO.

Remark 2. Many other SMC/SMDO designs in the literature also contain a preliminary feedback term using NDI to reduce the control efforts of SMC/SMDO. For example, adaptive fuzzy gain-scheduling SMC [12], first-order SMC using the equivalent control estimated from the nominal model [4,6–9,19], adaptive SMC [5], higher-order SMC [20–22], adaptive super-twisting SMC [11], modified super-twisting SMC using a higher-order sliding mode observer [13].

One well-known drawback of NDI is its model dependency, which consequently reduces its robustness to model uncertainties, on-board faults and external disturbances. SMC/SMDO is able to observe and compensate for bounded perturbations, as shown in Eqs. (9, 10). Even though the SMC/SMDO control input designed by Eq. (10) is continuous, the high-frequency switchings of v_o are only attenuated by filtering, instead of being totally rejected [19]. In other words, the $\hat{v}_{\text{eq}}$ term in Eq. (10) is still oscillating. A method that can simultaneously reduce the model dependency of NDI and mitigate the side effects of SMC/SMDO would be beneficial.

2.2. INDI-SMC/SMDO

INDI-SMC/SMDO aims to reduce the model dependency, and improve the robustness of NDI-SMC/SMDO, without using high control/observer gains. Denote the sampling interval as Δt. To begin with, the incremental dynamic equation is derived by taking the first-order Taylor series expansion of Eq. (1) around the condition at $t - \Delta t$ (denoted by the subscript 0) as:

$$\begin{aligned}\dot{y} &= \dot{y}_0 + G(x_0, \kappa_0)\Delta u + \frac{\partial[f(x,\kappa) + G(x,\kappa)u]}{\partial x}\bigg|_0 \Delta x\\ &\quad + \frac{\partial[f(x,\kappa) + G(x,\kappa)u]}{\partial\kappa}\bigg|_0 \Delta\kappa\\ &\quad + \Delta d + \mathcal{O}(\Delta x^2) \triangleq \dot{y}_0 + G(x_0, \kappa_0)\Delta u + \Delta d + \delta(x, \kappa, \Delta t)\end{aligned} \tag{12}$$

In the above equation, $\Delta x = x - x_0$, $\Delta u = u - u_0$, respectively denote the variations of states and control inputs in one incremental time step Δt. $\Delta\kappa = \kappa - \kappa_0$ denotes the changes of the fault indicator κ, while $\Delta d = d - d_0$ denotes the variations of the external disturbances d in Δt. $\dot{y}_0$ is the latest sampled output derivate vector. If $\dot{y}_0$ cannot be measured, it can be estimated from the sampled outputs. The approaches of obtaining $\dot{y}_0$ for control implementation will be further discussed in Sec. 5. The remainder term $\mathcal{O}(\Delta x^2)$ is only a function of Δx^2, since according to Eqs. (1, 2), $\frac{\partial^i\dot{y}}{\partial u^i} = 0$, $\frac{\partial^i\dot{y}}{\partial d^i} = 0$, $\frac{\partial^i\dot{y}}{\partial\kappa^i} = 0$ for all $i \geq 2$. It is noteworthy that, compared to the incremental dynamic equations derived in [28,24], Eq. (12) takes partial derivatives with respect to both κ and d.

The same sliding variable σ in Eq. (3) is also used by INDI-SMC/SMDO for fair comparisons. However, the controller will be designed based on Eq. (12) instead of Eq. (1). The dynamics of σ are then derived as:

$$\begin{aligned}\dot{\sigma} &= \dot{e} + K_c e = (\dot{y}_c + K_c e - \dot{y}_0) + (-\delta(x, \kappa, \Delta t) - \Delta d)\\ &\quad - \bar{G}\Delta u - (G - \bar{G})\Delta u\\ &\triangleq \bar{\Psi}' + \Delta\Psi' - \bar{G}\Delta u - \Delta G\Delta u\end{aligned} \tag{13}$$

Design an auxiliary sliding variable $s' = \sigma + z'$, $\dot{z}' = -\bar{\Psi}' + \bar{G}\Delta u - v'_o$, then by using Eq. (13), the dynamics of s' are:

$$\dot{s}' = (\Delta\Psi' - \Delta G\Delta u) - v'_o \triangleq -\varepsilon_{indi} - v'_o \quad (14)$$

ε_{indi} in Eq. (14) is the lumped perturbation term in INDI-SMC/SMDO. Denote the control input as u_{indi}, which will be designed in Theorem 1. Using Eq. (2), $\delta(x, \kappa, \Delta t)$ in Eq. (12) is further derived as:

$$\delta(x, \kappa, \Delta t) = \delta_b(x, \Delta t) + \delta_d(x, \Delta t)\kappa_0 + \delta_\kappa(x)\Delta\kappa \quad (15)$$

where

$$\delta_b(x, \Delta t) = \frac{\partial[\bar{f} + \hat{f} + (\bar{G} + \hat{G})u_{indi}]}{\partial x}\bigg|_0 \Delta x + \mathcal{O}(\Delta x^2)$$

$$\delta_d(x, \Delta t) = \frac{\partial[(f_f - \bar{f}) + (G_f - \bar{G})u_{indi}]}{\partial x}\bigg|_0 \Delta x$$

$$\delta_\kappa(x) = [(f_f - \bar{f}) + (G_f - \bar{G})u_{indi}]|_0 \quad (16)$$

Therefore, recall Eq. (13), ε_{indi} in Eq. (14) is written as:

$$\begin{aligned}\varepsilon_{indi} &= -\Delta\Psi' + \Delta G\Delta u_{indi} \\ &= [\delta_b + \hat{G}\Delta u_{indi} + \Delta d] + \kappa_0\delta_d + \kappa(G_f - \bar{G})\Delta u_{indi} + \delta_\kappa\Delta\kappa \end{aligned} \quad (17)$$

For a bounded ε_{indi}, design v'_o in Eq. (14) as:

$$v'_o = K'_s\text{Sign}(s') = [K'_{s,1}\text{sign}(s'_1), K'_{s,2}\text{sign}(s'_2), ..., K'_{s,n}\text{sign}(s'_n)]^T,$$

$$K'_{s,i} \geq \eta + |\varepsilon_{indi,i}| \quad (18)$$

where η is a small positive constant.

Theorem 1. *For system described by Eqs. (1, 2), and the sliding variable σ in Eq. (3), if the INDI-SMC/SMDO control is designed as*

$$\Delta u_{indi} = \bar{G}^{-1}(\bar{\Psi}' + K'_\sigma\sigma + \hat{v}'_{eq}) \quad (19)$$

where $\bar{\Psi}'$ is defined in Eq. (13), $K'_\sigma = \text{diag}\{K'_{\sigma,i}\}$, $K'_{\sigma,i} > 0$, and $\hat{v}'_{eq}$ is low-pass filtered from v'_o in Eq. (18), then under Assumption 1, for a bounded ε_{indi} (Eq. (17)), σ will be ultimately bounded by an arbitrarily small bound.

Proof. Chose a candidate Lyapunov function $V_3 = \frac{1}{2}s'^T s'$, and use Eqs. (14, 18) lead to:

$$\begin{aligned}\dot{V}_3 = s'^T\dot{s}' = s'^T(-\varepsilon_{indi} - v'_o) &\leq \sum_{i=1}^n |s'_i||\varepsilon_{indi,i}| - K'_{s,i}|s'_i| \\ &\leq -\eta\sum_{i=1}^n |s'_i| \end{aligned} \quad (20)$$

Therefore, according to the η reaching law [19,18], the sliding surfaces $s'_i = 0$, $i = 1, 2, ..., n$ are reached in finite time $t'_{r,i} \leq |s'_i(0)|/\eta$. On the sliding surfaces, using Eq. (14), the equivalent control [2,19] $v'_{eq,i}$ equals $-\varepsilon_{indi,i}$. This equivalent control can be estimated by filtering v'_o as $\hat{v}'_{eq,i}(s) = G_{LPF}(s)v'_{o,i}(s)$, where $G_{LPF}(s)$ is the transfer function of a low-pass filter. Consequently, $\hat{v}'_{eq,i}$ estimates $-\varepsilon_{indi,i}$ in finite time with a small estimation error proportional to the time constant of the filter, i.e. $|-\varepsilon_{indi,i} - \hat{v}'_{eq,i}| < \mathcal{O}(\tau_i)$. In a vector form, $\|\varepsilon_{indi} + \hat{v}'_{eq}\| < \mathcal{O}(\tau) \triangleq \|[\mathcal{O}(\tau_1), ..., \mathcal{O}(\tau_n)]^T\|$.

Use the observed perturbation term $\hat{v}'_{eq}$, and substitute Eqs. (17, 19) into Eq. (13) result in:

$$\dot{\sigma} = -K'_\sigma\sigma + [\Delta\Psi' - \Delta G\Delta u_{indi}] - \hat{v}'_{eq} = -K'_\sigma\sigma - (\varepsilon_{indi} + \hat{v}'_{eq}) \quad (21)$$

Introduce a candidate Lyapunov function $V_4 = \sigma^T P'\sigma$, where $P' = P'^T > 0$ is the solution of the Lyapunov equation $P'K'_\sigma + K'^T_\sigma P' = I$. Then when $t > \max\{t'_{r,i}\}$, the time derivative of V_4 is:

$$\begin{aligned}\dot{V}_4 &= -\sigma^T[P'K'_\sigma + K'^T_\sigma P']\sigma - 2\sigma^T P'(\varepsilon_{indi} + \hat{v}'_{eq}) \\ &< -\|\sigma\|^2 + 2\|\sigma\|\|P'\|\mathcal{O}(\tau) \\ &\leq -\gamma\|\sigma\|^2, \quad \forall\|\sigma\| \geq \frac{2\|P'\|\mathcal{O}(\tau)}{1-\gamma} \end{aligned} \quad (22)$$

with constant $\gamma \in (0, 1)$. Eq. (22) proves σ is ultimately bounded by a class $\mathcal{K}$ function [24,34] of $\mathcal{O}(\tau)$. In theory, this ultimate bound can be made arbitrarily small [19,31] by reducing τ_i and increasing $K'_{\sigma,i}$. □

The total control command of INDI-SMC/SMDO is $u_{indi} = u_{indi}|_0 + \Delta u_{indi}$, where Δu_{indi} is designed as Eq. (19), $u_{indi}|_0$ is the latest sampled u_{indi}. If $u_{indi}|_0$ is not directly measurable, it can also be estimated online [35]. In view of Eqs. (13, 19), the control law designed using the structure of INDI does not require the model information of f. Even through the model dependency of INDI-SMC/SMDO is reduced, its robustness is enhanced by virtue of its sensor-based structure [24,28,36]. This distinguishes INDI-SMC/SMDO from Ref. [37,38], where the nominal model of f is still needed. The sensor-based structure also has lower computation load than the online dynamic reconstruction using neural networks [39]. Apart from its reduced model dependency, other benefits of using the INDI control structure in SMC/SMDO designs will be further explored.

For both NDI and INDI based SMC/SMDO, the boundedness of the perturbation term is the precondition of controller design. The boundedness of ε_{ndi} for all t is assumed in Assumption 2. Instead of making a similar assumption for ε_{indi}, it will be shown in Theorem 2 that some less strict conditions can guarantee the boundedness of ε_{indi}.

Assumption 3. The partial derivatives of f and G in Eq. (1) with respect to x, up to any order, are bounded.

Assumption 4. $\delta_\kappa(x)$ in Eq. (16) is bounded for $t_f \leq t < t_f + \Delta t$.

Assumption 4 is less strict than Assumption 2. It can be seen from Eqs. (7, 16) that the $\kappa[(f_f - \bar{f}) + (G_f - \bar{G})u_{ndi}]$ term contained in ε_{ndi} corresponds to $\delta_\kappa(x)$ in ε_{indi}. However, only the boundedness of $\delta_\kappa(x)$ for a short time interval Δt is needed in Assumption 4, while the boundedness of the entire ε_{ndi} for all t is required in Assumption 2. Since $\kappa(t)$ is a step function to indicate a sudden fault, $\Delta\kappa$ is a single square pulse with magnitude of one and width of Δt. Consequently, the term $\delta_\kappa(x)\Delta\kappa$ is only non-zero during a short time interval $t_f \leq t < t_f + \Delta t$. After $t = t_f + \Delta t$, the main influences of the fault have already been included by the measurements/estimations at the latest sampled condition.

Theorem 2. *If $\|I - G\bar{G}^{-1}\| \leq \bar{b} < 1$ for all t, under Assumptions 3 and 4, for sufficiently high sampling frequency, ε_{indi} given by Eq. (17) is ultimately bounded.*

Proof. Using Eqs. (13, 17, 19), ε_{indi} is written as

$$\begin{aligned}\varepsilon_{indi} &= \delta(x, \kappa, \Delta t) + \Delta d + \Delta G\bar{G}^{-1}(\bar{\Psi}' + K'_\sigma\sigma + \hat{v}'_{eq}) \\ &= \delta(x, \kappa, \Delta t) + \Delta d + (G\bar{G}^{-1} - I)((\dot{y}_c + K_c e) \\ &\quad + K'_\sigma\sigma + \hat{v}'_{eq} - \dot{y}_0) \end{aligned} \quad (23)$$

Define the lumped virtual control term as $\boldsymbol{v} = (\dot{\boldsymbol{y}}_c + \boldsymbol{K}_c \boldsymbol{e}) + \boldsymbol{K}'_\sigma \boldsymbol{\sigma} + \hat{\boldsymbol{v}}'_{\text{eq}}$, which contains three parts: the classical INDI virtual control $\dot{\boldsymbol{y}}_c + \boldsymbol{K}_c \boldsymbol{e}$, the SMC virtual control $\boldsymbol{K}'_\sigma \boldsymbol{\sigma}$, and the observation term $\hat{\boldsymbol{v}}'_{\text{eq}}$. These three terms are all continuous in time.

Using the definition $\boldsymbol{\sigma} = \boldsymbol{e} + \boldsymbol{K}_c \int \boldsymbol{e}\mathrm{d}t$, $\boldsymbol{e} = \boldsymbol{y}_c - \boldsymbol{y}$, and the closed-loop dynamics given by Eq. (21), then

$$\dot{\boldsymbol{\sigma}} = -\boldsymbol{K}'_\sigma \boldsymbol{\sigma} - (\boldsymbol{\varepsilon}_{\text{indi}} + \hat{\boldsymbol{v}}'_{\text{eq}}) = \dot{\boldsymbol{y}}_c - \dot{\boldsymbol{y}} + \boldsymbol{K}_c \boldsymbol{e} \qquad (24)$$

Therefore

$$\dot{\boldsymbol{y}} = (\dot{\boldsymbol{y}}_c + \boldsymbol{K}_c \boldsymbol{e}) + \boldsymbol{K}'_\sigma \boldsymbol{\sigma} + \hat{\boldsymbol{v}}'_{\text{eq}} + \boldsymbol{\varepsilon}_{\text{indi}} = \boldsymbol{v} + \boldsymbol{\varepsilon}_{\text{indi}} \qquad (25)$$

Eq. (25) is valid for all t, thus for the previous time step, $\dot{\boldsymbol{y}}_0 = \boldsymbol{v}_0 + \boldsymbol{\varepsilon}_{\text{indi}_0}$. Substituting this equation into Eq. (23) yields:

$$\begin{aligned}
\boldsymbol{\varepsilon}_{\text{indi}} &= \delta(\boldsymbol{x}, \kappa, \Delta t) + \Delta \boldsymbol{d} + (\boldsymbol{G}\bar{\boldsymbol{G}}^{-1} - \boldsymbol{I})(\boldsymbol{v} - \dot{\boldsymbol{y}}_0) \\
&= (\boldsymbol{I} - \boldsymbol{G}\bar{\boldsymbol{G}}^{-1})\boldsymbol{\varepsilon}_{\text{indi}_0} - (\boldsymbol{I} - \boldsymbol{G}\bar{\boldsymbol{G}}^{-1})(\boldsymbol{v} - \boldsymbol{v}_0) \\
&\quad + \delta(\boldsymbol{x}, \kappa, \Delta t) + \Delta \boldsymbol{d} \\
&\triangleq \boldsymbol{E}\boldsymbol{\varepsilon}_{\text{indi}_0} - \boldsymbol{E}\Delta \boldsymbol{v} + \delta(\boldsymbol{x}, \kappa, \Delta t) + \Delta \boldsymbol{d}
\end{aligned} \qquad (26)$$

which can be written in a recursive way as:

$$\boldsymbol{\varepsilon}_{\text{indi}}(k) = \boldsymbol{E}(k)\boldsymbol{\varepsilon}_{\text{indi}}(k-1) - \boldsymbol{E}(k)\Delta \boldsymbol{v}(k) + \delta(k) + \Delta \boldsymbol{d}(k) \qquad (27)$$

k in the above equation indicates the k-th time step. Since $\boldsymbol{x}$ is continuously differentiable, $\lim_{\Delta t \to 0} \|\Delta \boldsymbol{x}\| = 0$. Therefore, using Assumption 3, the perturbation terms satisfy:

$$\lim_{\Delta t \to 0} \|\delta_b(\boldsymbol{x}, \Delta t)\| = 0, \quad \lim_{\Delta t \to 0} \|\delta_d(\boldsymbol{x}, \Delta t)\| = 0, \quad \forall \boldsymbol{x} \in \mathcal{R}^n \qquad (28)$$

which means that the norms of these perturbation terms become negligible for sufficiently small sampling interval [24,28]. Eq. (28) also indicates that $\forall \bar{\delta}_\varepsilon > 0, \exists \overline{\Delta t} > 0, s.t. \ \forall \Delta t \in (0, \overline{\Delta t}], \ \forall \boldsymbol{x} \in \mathcal{R}^n, \ \|\delta_b(\boldsymbol{x}, \Delta t)\| \leq \bar{\delta}_\varepsilon, \ \|\delta_d(\boldsymbol{x}, \Delta t)\| \leq \bar{\delta}_\varepsilon$. In other words, there exists a Δt that ensures the boundedness of both $\delta_b(\boldsymbol{x}, \Delta t)$ and $\delta_d(\boldsymbol{x}, \Delta t)$. Also, these bounds can be further diminished by reducing the sampling interval. Moreover, since $\Delta \kappa$ is only non-zero for $t_f \leq t < t_f + \Delta t$, then $\delta_\kappa \Delta \kappa$ is bounded under Assumption 4. Recall Eq. (15), since $\|\delta(\boldsymbol{x}, \kappa, \Delta t)\| \leq \|\delta_b(\boldsymbol{x}, \Delta t)\| + \|\delta_d(\boldsymbol{x}, \Delta t)\| \cdot 1 + \|\delta_\kappa(\boldsymbol{x})\Delta \kappa\|$, then Assumptions 3, 4 and a sufficiently small Δt ensure a bounded $\delta(\boldsymbol{x}, \kappa, \Delta t)$. Denote the bound as $\bar{\delta}$. Furthermore, $\boldsymbol{v}$ is designed to be continuous in time, thus

$$\lim_{\Delta t \to 0} \|\boldsymbol{v} - \boldsymbol{v}_0\| = 0, \quad \forall \boldsymbol{x} \in \mathcal{R}^n \qquad (29)$$

consequently, for a sufficient small Δt, $\Delta \boldsymbol{v} = \boldsymbol{v} - \boldsymbol{v}_0$ is bounded. Denote this bound as $\overline{\Delta v}$. In addition, for a bounded disturbance vector $\boldsymbol{d}$, its increment in one time step $\Delta \boldsymbol{d}$ is also bounded. Denote this bound as $\overline{\Delta d}$. Using these bounds, and recall the condition $\|\boldsymbol{E}\| = \|\boldsymbol{I} - \boldsymbol{G}\bar{\boldsymbol{G}}^{-1}\| \leq \bar{b} < 1$ in this theorem, Eq. (27) satisfies:

$$\begin{aligned}
\|\boldsymbol{\varepsilon}_{\text{indi}}(k)\| &\leq (\bar{b})^k \|\boldsymbol{\varepsilon}_{\text{indi}}(0)\| + \sum_{j=1}^{k} (\bar{b})^{k-j+1} \|\Delta \boldsymbol{v}(j)\| \\
&\quad + \sum_{j=1}^{k-1} (\bar{b})^{k-j} \|\delta(j) + \Delta \boldsymbol{d}(j)\| + \|\delta(j) + \Delta \boldsymbol{d}(j)\| \\
&\leq (\bar{b})^k \|\boldsymbol{\varepsilon}_{\text{indi}}(0)\| + \overline{\Delta v} \sum_{j=1}^{k} (\bar{b})^{k-j+1} \\
&\quad + (\bar{\delta} + \overline{\Delta d}) \sum_{j=1}^{k-1} (\bar{b})^{k-j} + (\bar{\delta} + \overline{\Delta d})
\end{aligned}$$

$$= (\bar{b})^k \|\boldsymbol{\varepsilon}_{\text{indi}}(0)\| + \overline{\Delta v} \frac{\bar{b} - \bar{b}^{k+1}}{1 - \bar{b}} + (\bar{\delta} + \overline{\Delta d}) \frac{1 - \bar{b}^k}{1 - \bar{b}} \qquad (30)$$

Since $\bar{b} < 1$, Eq. (30) satisfies:

$$\|\boldsymbol{\varepsilon}_{\text{indi}}\| \leq \frac{\bar{b}\overline{\Delta v} + \bar{\delta} + \overline{\Delta d}}{1 - \bar{b}}, \quad \text{as } k \to \infty \qquad (31)$$

In conclusion, $\boldsymbol{\varepsilon}_{\text{indi}}$ is bounded for all k, and is ultimately bounded by $\frac{\bar{b}\overline{\Delta v} + \bar{\delta} + \overline{\Delta d}}{1 - \bar{b}}$. $\square$

Remark 3. Theorem 2 in this paper improves the Theorem 1 in [28] in three aspects: 1) consideration of the external disturbances $\boldsymbol{d}$; 2) consideration of the sudden faults, as $\delta(\boldsymbol{x}, \kappa, \Delta t)$ is a function of the fault indicator κ; 3) the virtual control $\boldsymbol{v}$ in this paper also includes the contributions from SMC and SMDO, while the $\boldsymbol{v}_c$ in [28] only considers the classical INDI virtual control term.

Remark 4. Theorem 2 proves that a diagonally dominate structure of $\boldsymbol{G}\bar{\boldsymbol{G}}^{-1}$, a sufficiently high sampling frequency, as well as Assumptions 3 and 4 guarantee a bounded $\boldsymbol{\varepsilon}_{\text{indi}}$. This bound can also be further diminished by increasing the sampling frequency. By contrast, $\boldsymbol{\varepsilon}_{\text{ndi}}$ is independent of Δt, and its boundedness is undetermined under the same conditions. Therefore, for the feasibility of the NDI-SMC/SMDO design, the stricter Assumption 2 needs to be imposed.

2.3. Comparisons between NDI and INDI based SMC/SMDO

A block diagram is shown by Fig. 1, in which two switches are used to transform between NDI and INDI based SMC/SMDO. When these switches are connected to black solid lines, the INDI-SMC/SMDO control structure is activated, where the controller uses the measurements/estimations of $\dot{\boldsymbol{y}}_0$ and $\boldsymbol{u}_{\text{indi}}|_0$. On the contrary, when the switches are connected to blue dashed lines, the NDI-SMC/SMDO control structure is activated, which depends on the model $\bar{\boldsymbol{f}}(\boldsymbol{x})$. This block diagram mainly illustrates the control structures, so the gain matrices $\boldsymbol{K}_\sigma$, $\boldsymbol{K}_s$ can be different for these two approaches.

As can be seen from the derivations of NDI and INDI based SMC/SMDO and Fig. 1, the same SMC/SMDO design is used to compensate for different perturbations, $\boldsymbol{\varepsilon}_{\text{ndi}}$ and $\boldsymbol{\varepsilon}_{\text{indi}}$. The properties of these perturbations are crucial to the stability and robustness of the closed-loop systems. As discussed in subsection 2.2, $\boldsymbol{\varepsilon}_{\text{indi}}$ is bounded when the conditions in Theorem 2 are satisfied, while the boundedness of $\boldsymbol{\varepsilon}_{\text{ndi}}$ is undetermined under the same conditions. Moreover, it has been proved in [28] that there exists a Δt such that $\boldsymbol{\varepsilon}_{\text{indi}}$ has smaller bound as compared to $\boldsymbol{\varepsilon}_{\text{ndi}}$. This feature of the incremental framework is fundamentally beneficial for reducing the switching gains in SMC [28]. However, only the model uncertainties are considered in [28]. In this paper, the properties of $\boldsymbol{\varepsilon}_{\text{ndi}}$ and $\boldsymbol{\varepsilon}_{\text{indi}}$ will be compared considering model uncertainties, external disturbances and sudden faults. Their influences on SMC/SMDO design will also be revealed.

Denote the fault instant as $t = t_f$, the values of $\boldsymbol{\varepsilon}_{\text{ndi}}$ and $\boldsymbol{\varepsilon}_{\text{indi}}$ will be analyzed in three cases:

1. Pre-fault $t < t_f$: $\kappa_0 = \kappa = 0$, $\Delta \kappa = 0$.
2. Fault instant $t_f \leq t < t_f + \Delta t$: $\kappa_0 = 0$, $\kappa = 1$, $\Delta \kappa = 1$.
3. Post-fault $t \geq t_f + \Delta t$: $\kappa_0 = \kappa = 1$, $\Delta \kappa = 0$.

For the pre-fault condition, recall Eqs. (7, 17), $\boldsymbol{\varepsilon}_{\text{ndi}} = \hat{\boldsymbol{f}} + \hat{\boldsymbol{G}}\boldsymbol{u}_{\text{ndi}} + \boldsymbol{d}$, while $\boldsymbol{\varepsilon}_{\text{indi}} = \delta_b + \hat{\boldsymbol{G}}\Delta \boldsymbol{u}_{\text{indi}} + \Delta \boldsymbol{d}$. $\|\hat{\boldsymbol{f}}\|$ is normally large because $\hat{\boldsymbol{f}}$ contains the uncertainties of inertia and aerodynamic
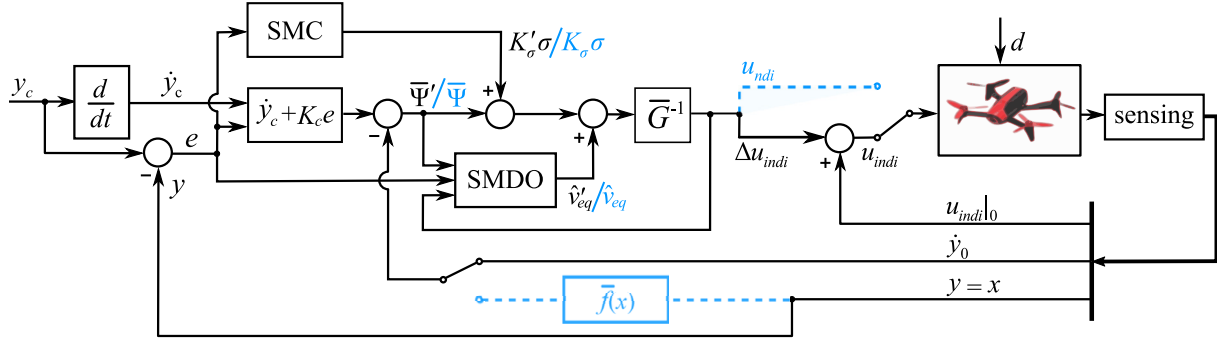
Fig. 1. Block diagram for INDI-SMC/SMDO (black solid lines) and NDI-SMC/SMDO (blue dashed lines).

properties for aerospace systems, which are the most challenging parts to model. On the contrary, as a function of Δt, $\|\boldsymbol{\delta}_b\|$ can become negligible as shown by Eq. (28). Also, when $\boldsymbol{u}_{\text{ndi}} \neq \boldsymbol{0}$, there exists a Δt that ensures $\|\hat{\boldsymbol{G}}\|\|\Delta \boldsymbol{u}_{\text{indi}}\| < \|\hat{\boldsymbol{G}}\|\|\boldsymbol{u}_{\text{ndi}}\|$ [24,28]. As compared to the fixed-wing aircraft control, this inequality is easier to fulfill in quadrotor control, because the control inputs (rotor speeds) are far from zero for overcoming gravity. Moreover, most external disturbances in real life are continuous, thus $\lim_{\Delta t \to 0} \|\boldsymbol{d}\| = 0$. In other words, when $\boldsymbol{d} \neq \boldsymbol{0}$, $\exists \Delta t, s.t. \|\Delta \boldsymbol{d}\| < \|\boldsymbol{d}\|$. For the discontinuous disturbances, such as a bird strike or a sudden collision, the influences of $\boldsymbol{d}$ can be analyzed in the same way as that of κ. In summary, when $t < t_f$, if $\boldsymbol{d} \neq \boldsymbol{0}$, $\boldsymbol{u}_{\text{ndi}} \neq \boldsymbol{0}$, there exists a Δt, such that the upper bound of $\boldsymbol{\varepsilon}_{\text{indi}}$ is smaller than that of $\boldsymbol{\varepsilon}_{\text{ndi}}$.

During $t_f \leq t < t_f + \Delta t$, $\kappa_0 = 0$, $\kappa = 1$, $\Delta \kappa = 1$. Recall Eqs. (7, 17), an additional term $(\boldsymbol{f}_f - \bar{\boldsymbol{f}}) + (\boldsymbol{G}_f - \bar{\boldsymbol{G}})\boldsymbol{u}_{\text{ndi}}$ is added to $\boldsymbol{\varepsilon}_{\text{ndi}}$, while $(\boldsymbol{G}_f - \bar{\boldsymbol{G}})\Delta \boldsymbol{u}_{\text{indi}} + \delta_\kappa$ is added to $\boldsymbol{\varepsilon}_{\text{indi}}$. Using the formulation of δ_κ (Eq. (16)), and the condition $\boldsymbol{u}_{\text{indi}} = \boldsymbol{u}_{\text{indi}}|_0 + \Delta \boldsymbol{u}_{\text{indi}}$, it can be seen that these two additional perturbation terms have comparable bounds.

When compared to the pre-fault condition, $\boldsymbol{\varepsilon}_{\text{ndi}}$ is augmented by $(\boldsymbol{f}_f - \bar{\boldsymbol{f}}) + (\boldsymbol{G}_f - \bar{\boldsymbol{G}})\boldsymbol{u}_{\text{ndi}}$ in the post-fault condition, while $\delta_d + (\boldsymbol{G}_f - \bar{\boldsymbol{G}})\Delta \boldsymbol{u}_{\text{indi}}$ is added to $\boldsymbol{\varepsilon}_{\text{indi}}$. As discussed in subsection 2.2, the $\delta_\kappa(\boldsymbol{x})\Delta \kappa$ term in $\boldsymbol{\varepsilon}_{\text{indi}}$ converges to zero after the fault. Even though the multiplicative uncertain term $(\boldsymbol{G}_f - \bar{\boldsymbol{G}})\Delta \boldsymbol{u}_{\text{indi}}$ still exists in $\boldsymbol{\varepsilon}_{\text{indi}}$, there exists a Δt that ensures $\|(\boldsymbol{G}_f - \bar{\boldsymbol{G}})\|\|\Delta \boldsymbol{u}_{\text{indi}}\| < \|(\boldsymbol{G}_f - \bar{\boldsymbol{G}})\|\|\boldsymbol{u}_{\text{ndi}}\|$, when $\boldsymbol{u}_{\text{ndi}} \neq \boldsymbol{0}$. Moreover, system using the INDI control structure is only perturbed by δ_d instead of $\boldsymbol{f}_f - \bar{\boldsymbol{f}}$. Recall Eq. (28), after the fault occurs, if $\boldsymbol{d} \neq \boldsymbol{0}$, $\boldsymbol{u}_{\text{ndi}} \neq \boldsymbol{0}$, there exists a Δt, such that the upper bound of $\boldsymbol{\varepsilon}_{\text{indi}}$ is smaller than that of $\boldsymbol{\varepsilon}_{\text{ndi}}$.

In summary, there exists a sampling interval Δt, such that in the perturbed circumstances, if $\boldsymbol{u}_{\text{ndi}} \neq \boldsymbol{0}$, the upper bound of $\boldsymbol{\varepsilon}_{\text{indi}}$ is smaller than that of $\boldsymbol{\varepsilon}_{\text{ndi}}$, before and after the fault. Also, the upper bound of $\boldsymbol{\varepsilon}_{\text{indi}}$ can be diminished by decreasing Δt. These properties of $\boldsymbol{\varepsilon}_{\text{indi}}$ can fundamentally reduce the control efforts of SMC/SMDO, because for most SMC and SMDO methods, the required switching gains are monotonically increasing functions of the uncertainty bounds. As a consequence, the SMC/SMDO designs based on the incremental control structure can achieve better performance and robustness using not only less model information but also reduced gains, as compared to those NDI based methods. The robustness of the incremental control structure is contributed by its sensor-based characteristic, that the uncertainties can be reduced by fully exploring the measurements.

It is worth noting that $\boldsymbol{\varepsilon}_{\text{indi}}$ also has smaller variations in different fault cases, while the augmented uncertainty term $(\boldsymbol{f}_f - \bar{\boldsymbol{f}}) + (\boldsymbol{G}_f - \bar{\boldsymbol{G}})\boldsymbol{u}_{\text{ndi}}$ in $\boldsymbol{\varepsilon}_{\text{ndi}}$ is more fault-case dependent. Therefore, INDI-SMC/SMDO has the potential of passively resisting a wider range of perturbations, while gain adjustments may be required by NDI-SMC/SMDO in different fault scenarios.
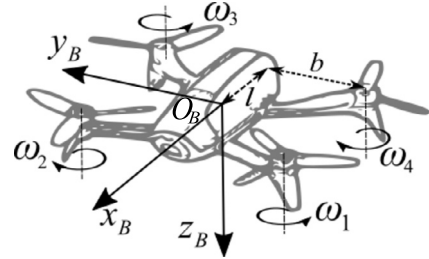

Fig. 2. A Bebop 2 quadrotor and axes definition.

The above analyses are conducted for generic nonlinear systems. The condition of "sufficiently high sampling frequency" may sound strict, but actually it is not difficult to find a reasonable Δt in practice. Further discussions about the selections of Δt can be found in [24]. In the following two sections, the benefits of INDI-SMC/SMDO will be demonstrated via both simulations and flight tests for a quadrotor fault tolerant control problem.

3. Quadrotor fault tolerant flight control

In order to compare the performance and robustness of NDI and INDI based SMC/SMDO, a quadrotor attitude control problem in the presence of model uncertainties, wind disturbances, and actuator faults will be considered in this section. The position control of quadrotors can be designed in the same way.

3.1. Quadrotor model

A Parrot Bebop 2 quadrotor is shown in Fig. 2. Denote the body frame as (O_B, X_B, Y_B, Z_B), where O_B coincides with the aircraft center of mass, and $O_B X_B Z_B$ represents the aircraft symmetrical plane. The distances to each of the rotors along the $O_B X_B$ and $O_B Y_B$ axes are respectively given by l and b. The rotation rates of the four rotors are denoted by $\boldsymbol{\omega} = [\omega_1, \omega_2, \omega_3, \omega_4]^T$. The orientation of the vehicle is described by Euler angles $\boldsymbol{\theta} = [\phi, \theta, \psi]^T$. Assume $\theta \in (-\frac{\pi}{2}, \frac{\pi}{2})$, $\phi \in (-\frac{\pi}{2}, \frac{\pi}{2})$. Expressing the angular rate of the quadrotor in the body frame as $\boldsymbol{\Omega} = [p, q, r]^T$, then the kinematic equations for the Euler angles are:

$$\dot{\boldsymbol{\theta}} = \boldsymbol{R}_\theta(\boldsymbol{\theta})\boldsymbol{\Omega} \tag{32}$$

in which $\boldsymbol{R}_\theta(\boldsymbol{\theta})$ can be found in [40]. The quadrotor rotational dynamics are given by:

$$\boldsymbol{I}_v(\kappa)\dot{\boldsymbol{\Omega}} + \boldsymbol{\Omega} \times \boldsymbol{I}_v(\kappa)\boldsymbol{\Omega} = \boldsymbol{M}_c(\boldsymbol{\omega}^2, \kappa) + \boldsymbol{M}_a(\boldsymbol{\Omega}, \boldsymbol{V}_a, \kappa)$$
$$+ \boldsymbol{M}_r(\boldsymbol{\omega}, \dot{\boldsymbol{\omega}}, \boldsymbol{\Omega}, \boldsymbol{I}_{r_{zz}}(\kappa)) \tag{33}$$

where $\boldsymbol{I}_v(\kappa)$ is the inertia matrix of the whole quadrotor, $\boldsymbol{M}_a(\boldsymbol{\Omega}, \boldsymbol{V}_a, \kappa)$ is the aerodynamic moment vector, $\boldsymbol{V}_a$ is the quadrotor

airspeed, $M_c(\omega^2, \kappa)$ is the control moment vector. $M_r(\omega, \dot{\omega}, \Omega,$ $I_{r_{zz}}(\kappa))$ contains two parts: the gyroscopic moments of the rotors (as a function of ω, Ω, rotor inertia vector $I_{r_{zz}}(\kappa)$), and also the spin-up torque of the rotors (as a function of $\dot{\omega}$ and $I_{r_{zz}}(\kappa)$). For the rotor failure cases considered in the present paper, the fault indicator κ is introduced to I_v, $I_{r_{zz}}$, M_c, M_a in Eq. (33). On the one hand, rotor failures directly lead to changes in the rotor inertia $I_{r_{zz}}$ and the inertia matrix of the whole quadrotor I_v. On the other hand, rotor failures modify the aerodynamic properties of the vehicle, thus the aerodynamic moment M_a and the control moment M_c are also functions of κ.

The thrust and reactive torque of the rotors are approximately proportional to ω^2 [26,41], and the proportionality coefficients are respectively denoted by k_i, λ_i, $i = 1, 2, 3, 4$. Therefore, using the geometry parameters shown in Fig. 2, M_c and the total thrust T can be modeled by:

$$\begin{pmatrix} M_c \\ \text{---} \\ T \end{pmatrix} = \begin{pmatrix} -bk_1 & bk_2 & bk_3 & -bk_4 \\ lk_1 & lk_2 & -lk_3 & -lk_4 \\ \lambda_1 & -\lambda_2 & \lambda_3 & -\lambda_4 \\ \text{-----} & \text{-----} & \text{-----} & \text{-----} \\ k_1 & k_2 & k_3 & k_4 \end{pmatrix} \omega^2 \triangleq G_m(\kappa)\omega^2 \quad (34)$$

The spin-up toque in M_r was neglected by most publications about quadrotor control, but it was shown in Ref. [26] via flight tests that this term is influential to the yaw channel control. However, if M_r is incorporated into the controller design, the system dynamics become $\dot{x} = f(x, \kappa) + G(x, \omega, \dot{\omega}, \omega^2, \kappa)$, which is not affine in ω. Actually, because the incremental dynamic equation is derived by taking partial derivatives with respect to u (Eq. (12)), the INDI control structure can also deal with non-affine in the control systems, as also shown in [26,24]. In spite of this benefit of INDI, for fair comparisons with NDI-SMC/SMDO, M_r is viewed as uncertainty in this paper, and will be observed by a SMDO. Consequently, the dynamic model for controller design becomes affine in ω^2.

3.2. Controller design

The control objective is quadrotor attitude command tracking, i.e. $\theta = [\phi, \theta, \psi]^T \to \theta_c$. Considering the natural time-scale separation of the quadrotor dynamics [8,26,27], the control law can be designed using two nested control loops. An alternative way is taking $y = \theta$, which makes the relative degree of y with respect to ω^2 equals two. Non-cascaded controllers can then be designed analogous to Eqs. (10, 19) [24]. Since these two approaches are analogous, and the cascaded control structure is more widely used in aerospace systems, this paper also designs the controllers in a cascaded way.

The inner-loop controller will be separately designed using NDI and INDI based SMC/SMDO methods, aiming at $\Omega \to \Omega_c$, $T \to T_c$, where Ω_c and T_c will be provided by the outer-loop controllers. In view of Eqs. (33, 34), the inner-loop dynamics are written as:

$$\begin{pmatrix} \dot{\Omega} \\ T/m \end{pmatrix} = \begin{pmatrix} -I_v^{-1}(\Omega \times I_v \Omega) + I_v^{-1} M_a \\ 0 \end{pmatrix} + \begin{pmatrix} I_v^{-1} & 0_{3\times1} \\ 0_{1\times3} & 1/m \end{pmatrix} G_m \omega^2 + \begin{pmatrix} d_1 + I_v^{-1} M_r \\ d_2 \end{pmatrix} \quad (35)$$

in which $d_1 \in \mathcal{R}^3$, $d_2 \in \mathcal{R}$ represent external disturbances.

Remark 5. In Ref. [4,5,7,9–12,14], the control input vector is taken as $u = [M_c, T]^T$. This choice is deficient because only the uncertainties of I_v can be considered in the controller designs. However, it is more difficult to estimate G_m owing to the aerodynamic effects. Furthermore, actuator faults have the largest influences on

G_m. In addition, for real-life implementations, $u = [M_c, T]^T$ still needs to be converted into rotor speed commands. Therefore, this paper takes $u = \omega^2$, and the rotor speed command vector is accordingly $\sqrt{u}$.

Define $x = [\Omega, \int (T/m) dt]^T$, then Eq. (35) can be expressed in the form of Eq. (1). Following the procedures in subsection 2.1, the inner-loop control using NDI-SMC/SMDO is designed by Eq. (10). On the other hand, the INDI-SMC/SMDO controller is designed using the incremental dynamic equation, which is derived as:

$$\begin{pmatrix} \dot{\Omega} \\ T/m \end{pmatrix} = \begin{pmatrix} \dot{\Omega}_0 \\ T_0/m \end{pmatrix} + \begin{pmatrix} \delta(\Omega, V_a, \kappa, \Delta t) \\ 0 \end{pmatrix} + \begin{pmatrix} I_v^{-1} & 0_{3\times1} \\ 0_{1\times3} & 1/m \end{pmatrix} G_m \Delta\omega^2 + \begin{pmatrix} \Delta d_1 + \delta_{M_r}(\Delta t) \\ \Delta d_2 \end{pmatrix}$$
$$(36)$$

where

$$\delta(\Omega, V_a, \kappa, \Delta t) = \frac{\partial[I_v^{-1}(-\Omega \times I_v\Omega + M_a)]}{\partial\Omega}\bigg|_0 \Delta\Omega$$
$$+ \frac{\partial[I_v^{-1}M_a]}{\partial V_a}\bigg|_0 \Delta V_a + \mathcal{O}(\Delta\Omega^2, \Delta V_a^2)$$
$$+ \frac{\partial[I_v^{-1}(-\Omega \times I_v\Omega + M_a + M_c)]}{\partial\kappa}\bigg|_0 \Delta\kappa \quad (37)$$

and with $\delta_{M_r}(\Delta t)$ representing the variations of $I_v^{-1} M_r$ in one incremental time step. According to the physical time-scale separations of quadrotor dynamics, the variations of velocities are slower than the variations of angular rates. Also, V_a is a continuous function of time. Based on the above two reasons, Eq. (28) is still valid. Following the procedures in subsection 2.2, the inner-loop control using INDI-SMC/SMDO is then designed by Eq. (19).

After the design of the inner-loop controllers using both NDI and INDI based SMC/SMDO, the outer-loop controllers are designed to provide the commands Ω_c and T_c. Ω_c is designed to achieve attitude control: $\theta \to \theta_c$, while T_c is designed to control height: $h \to h_c$.

Recall Eq. (32), since there is no model uncertainty in this kinematic equation, a simple NDI controller can be adopted. Design the virtual control as $v_{att} = \dot{\theta}_c + K_{att}(\theta_c - \theta)$, $K_{att} = \text{diag}\{K_{att_i}\}$, $K_{att_i} > 0$, $i = 1, 2, 3$, then the reference for the angular rates is designed as $\Omega_c = R_\theta^{-1}(\theta)v_{att}$. $R_\theta(\theta)$ is invertible when $\theta \in (-\frac{\pi}{2}, \frac{\pi}{2})$.

For the height control, define the position vector as $P = [x, y, -h]^T$, then its dynamics are given as:

$$\ddot{P} = g + R_{IB}(F_a + T)/m \quad (38)$$

where $g = [0, 0, g]^T$ is the gravitational acceleration vector, R_{IB} is the rotational matrix from the body frame to the inertial frame. F_a is the aerodynamic force vector expressed in the body frame, and $T = [0, 0, -T]^T$ is the thrust vector. Denote the z component of $\ddot{P}$ as a_z, and assume the aerodynamic force in the $O_B Z_B$ direction is negligible as compared to thrust, then the last row of Eq. (38) is written as $a_z = g - (\cos\theta\cos\phi)T/m$. Design the command for a_z as $a_{z_c} = -\ddot{h}_c - K_d(\dot{h}_c - \dot{h}) - K_p(h_c - h)$, $K_d > 0$, $K_p > 0$, then the command for thrust is accordingly given by $(T_c/m) = (g - a_{z_c})/(\cos\theta\cos\phi)$.

At this point, the height, attitude, and angular rate controllers have been completely designed. In order to enforce the natural time-scale separations in the closed-loop system, the gain matrices K_c, K_{att}, need to fulfill $\min(K_{c_i}) > \max(K_{att_i})$ for roll, pitch, and yaw control channels.
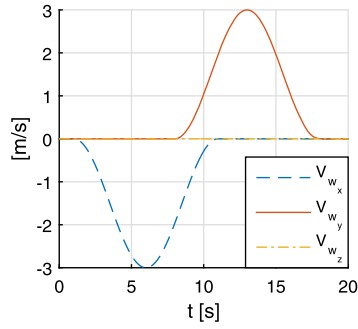
Fig. 3. Wind disturbances.

4. Numerical validations

In this section, the controllers designed in Sec. 2 and Sec. 3 will be tested in the Matlab/Simulink environment. Two models for a Parrot Bebop quadrotor are set up. One high fidelity model identified from wind tunnel test data [41] is used for simulations. Another simplified model, which excludes aerodynamic effects, gyroscopic moments and spin-up torque, is used by the controllers. It is worth noting that neglecting these factors in quadrotor control design is a common practice. The actuator dynamics are modeled as first-order low-pass filters with time constants of 0.02 s. The maximum and minimum rotational speed of the rotors are 12000 revolutions per minute (rpm) and 3000 rpm respectively. The controller sampling frequency is 500 Hz.

Three perturbation sources are tested: model uncertainties, wind disturbances and sudden actuator faults during flight.

For the model uncertainties, the inertia matrix $\bar{I}_v$ used by onboard controllers equals 70% of the nominal I_v. The mismatch between I_v and $\bar{I}_v$ brings model uncertainties to both f and G. The G_m matrix used for simulations is time varying because k_i, λ_i, $i = 1, 2, 3, 4$ are influenced by the aerodynamic conditions (airspeed, air density, etc.). However, for the simplicity of implementation, constant $\bar{G}_m$ matrix evaluated at the hover condition is used by the controllers, which brings model mismatches even without actuator fault.

Remark 6. The pure INDI control designed for a quadrotor in Ref. [26] identifies the time varying control effectiveness matrix during flight. This system identification based adaption is a modular approach, whose stability cannot be ensured. The usage of constant control effectiveness matrix in this paper is simpler, and the corresponding uncertainties can be compensated by SMC/SMDO.

The airspeed V_a of a quadrotor equals $V - V_w$ [40], where V is the ground speed, and V_w denotes the velocity of the atmosphere relative to the inertial frame. In this paper, V_w is considered as the "1-cos" gust [42]. As shown in Fig. 3, gusts are added along the x and y directions of the inertial frame. The maximum gust velocity equals 3 m/s. Since the airspeed V_a contains V_w, the dynamic pressure and the angle of attack of the rotor system are influenced by V_w. Consequently, the thrust, in-plane forces, and moments on each rotor are affected by V_w. As mentioned in Sec. 3, these aerodynamic effects caused by V_w are viewed as external disturbances. For more details about the influences of atmospheric disturbances on the quadrotors, readers are recommended to Ref. [29].

Finally, to model a sudden fault of the i-th rotor during flight, for $t \geq t_f$, the corresponding effectiveness in G_m is scaled in the simulation model, i.e. $k_i' = \mu_i k_i$, $\lambda_i' = \mu_i \lambda_i$, $\mu_i \in (0, 1]$. However, in spite of faults, constant $\bar{G}_m$ matrix is consistently used by both controllers.

The attitude commands are smoothly combined sigmoid functions (shown in Fig. 4 and Fig. 8) as continuous realizations of doublet signals. These commands on different channels have phase shifts with each other, in which way the decoupling performance of the controllers can be tested. The height command is $h = 1$ m. The initial conditions are $\phi(t = 0) = 0°$, $\theta(t = 0) = 0°$, $\psi(t = 0) = 0°$, $h(t = 0) = 0$ m.

The main focus of this paper is on the comparisons between NDI and INDI based SMC/SMDO designs, so the outer-loop controllers are kept identical. The gains used by the outer-loop controllers are: $K_p = 10$, $K_d = 5$, $K_{att} = \text{diag}([2, 2, 1])$, $K_c = \text{diag}([8, 8, 6])$. Trade-offs should be made when tuning the inner-loop parameters: K_σ, K_s, and the filter time constants τ_i. High K_σ gains can accelerate the convergence of σ, but will amplify measurement noise at the meanwhile. Trade-offs also exist in tuning the filter parameters in SMDO. Specifically, high cut-off frequency introduces more chattering and noise into $\hat{v}_{eq}$, but low cut-off frequency increases the observation errors $\mathcal{O}(\tau_i)$. For fair comparison, $K_\sigma = \text{diag}([0.5, 0.5, 0.5, 1])$, and $\tau = [0.05, 0.05, 0.08, 0.05]^T$ are used by both NDI and INDI based SMC/SMDO controllers. The filter time constant in the yaw channel is larger for suppressing the oscillations caused by the spin-up torque.

The gain requirements presented in Eqs. (8, 18) are the minimum possible gains for enforcing sliding motions [15–18]. Since ε_{ndi} and ε_{indi} are time-varying, the minimum possible gains are also time-varying. The dual layer nested adaptive methodology in [18] can be used to adjust the gains online. In subsection 2.3, it has been shown that there exists a Δt, the upper bound of ε_{indi} is smaller than that of ε_{ndi} in the presence of model uncertainties, wind disturbances, and sudden faults. Moreover, ε_{indi} also has smaller variations in different fault cases. Because of these merits, the required K_s gains for INDI-SMC/SMDO are lower and need less adjustments. For the simplicity of implementation, constant K_s gains will be used by both NDI and INDI based SMC/SMDO. In the following two subsections, the robustness and chattering magnitude of the two methods will be compared.

4.1. Simulation results of NDI-SMC/SMDO

Fig. 4 illustrates the tracking performance of NDI-SMC/SMDO. In all of the three different cases, model uncertainties and wind disturbances are incorporated, while the degree of actuator faults varies. Without loss of generality, sudden effectiveness losses are imposed on the third rotor at $t = 5$ s, which are reflected by the abrupt tracking overshoots in Fig. 4. Regardless of these overshoots, the quadrotor using NDI-SMC/SMDO control is able to recover from faults within seconds, and resist the perturbations of model uncertainties and wind disturbances at the same time. However, the tracking and decoupling performance of this controller indeed deteriorates with the increases of fault degree.

The responses of the sliding variables σ are shown in Fig. 5, as consistent with the analyses in Sec. 2, σ asymptotically converges to the sliding surface. Additionally, $\|\sigma\|$ distinctly increases after the actuator fault occurs, and $\|\sigma\|$ is positively correlated to the fault degree. It can also be observed from Fig. 5 that the auxiliary sliding variable s converges in finite time under perturbations. The high frequency switchings of s (which is normal [19]) will not influence the continuity of u because of the filtering process in SMDO.

One core parameter that guarantees the convergence of s is K_s. As proved by Eqs. (8, 9), the elements of K_s need to be larger than the uncertainty bounds. In view of Eq. (7) and the discussions in subsection 2.3, the uncertain term ε_{ndi} is influenced by all the three perturbation sources. Moreover, owing to the term $(f_f - \bar{f}) + (G_f - \bar{G})u_{ndi}$, $\|\varepsilon_{ndi}\|$ varies significantly for different fault
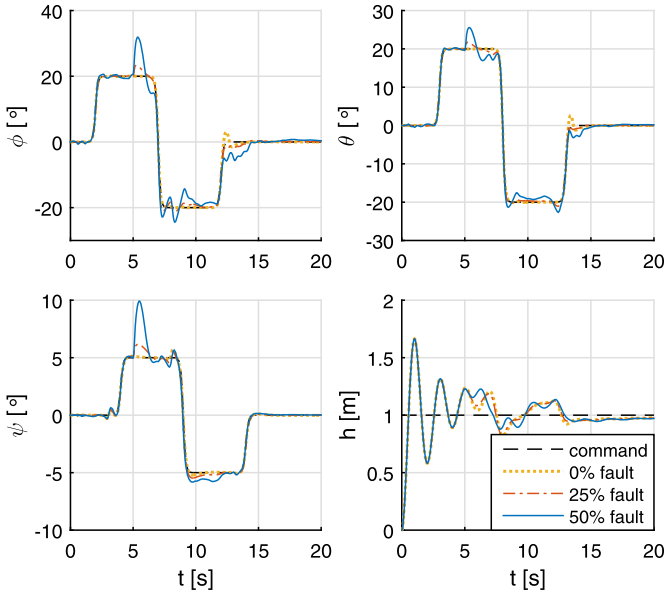
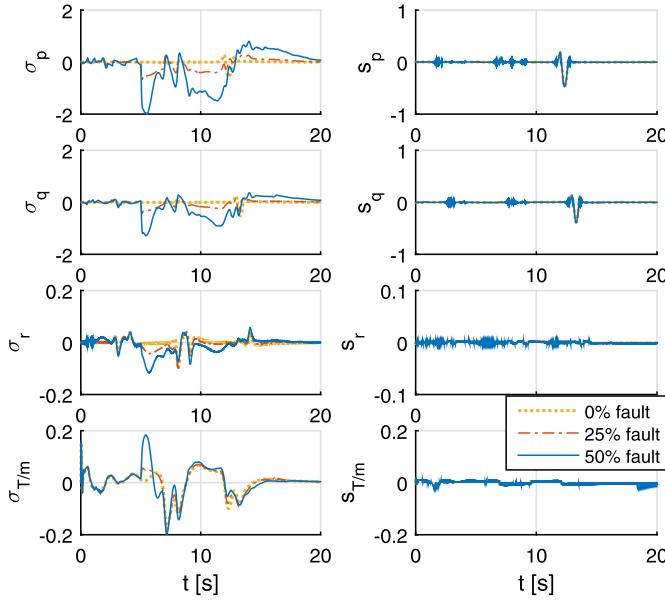**Fig. 4.** Quadrotor responses under NDI-SMC/SMDO control.

Fig. 5. Responses of sliding variables under NDI-SMC/SMDO control.

Fig. 6. Observed uncertainties $\hat{\boldsymbol{v}}_{eq}$ under NDI-SMC/SMDO control.

Fig. 7. Measured rotor speeds under NDI-SMC/SMDO control in the '50% fault' case.

4.2. Simulation results of INDI-SMC/SMDO

In this subsection, the same fault scenarios will be used to test the effectiveness of INDI-SMC/SMDO.

When comparing Fig. 8 with Fig. 4, obvious tracking performance improvements of INDI based control can be observed. The effectiveness of INDI-SMC/SMDO is hardly influenced by the perturbations, and only small ripples appear after $t = 5$ s.

The responses of the sliding variables in Fig. 9 also show improvements when compared to the responses in Fig. 5. Specifically, $|\sigma_p|$, $|\sigma_q|$ under INDI-SMC/SMDO are one order of magnitude smaller than the values using NDI-SMC/SMDO control. Moreover, $\boldsymbol{\sigma}$ in Fig. 9 has a higher convergence rate, and smaller variations. The auxiliary sliding variable $\boldsymbol{s}$ also shows smaller fluctuations in Fig. 9.

The main reason for the performance and robustness improvements of INDI based SMC/SMDO can be seen from Fig. 10. Since $\boldsymbol{s}$ in both Fig. 5 and Fig. 9 converges, $\hat{\boldsymbol{v}}_{eq}$ in Fig. 6 and Fig. 10 can respectively estimate $-\boldsymbol{\varepsilon}_{ndi}$ and $-\boldsymbol{\varepsilon}_{indi}$. According to the analyses in subsection 2.3, the upper bound of $\boldsymbol{\varepsilon}_{indi}$ is smaller than that of $\boldsymbol{\varepsilon}_{ndi}$ in the presence of faults, model uncertainties and disturbances. This is verified by comparing Fig. 10 with Fig. 6, where $|v_{eq,p}|$ and $|v_{eq,q}|$ are two orders of magnitude smaller under INDI based SMC/SMDO control than NDI based in the '50% fault' case. Also, $|v_{eq,r}|$ and $|v_{eq,T/m}|$ are one order of magnitude smaller under INDI-SMC/SMDO control. Furthermore, as illustrated in Fig. 10, since $\delta_\kappa(\boldsymbol{x})\Delta\kappa$ is only non-zero for $t_f \leq t < t_f + \Delta t$ (subsection 2.3), $\boldsymbol{\varepsilon}_{indi}$ has comparable bounds before and after a sudden fault. Furthermore, according to Eq. (17), after a fault oc-

cases. This is verified by Fig. 6, which presents abrupt increases of $\|\boldsymbol{\varepsilon}_{ndi}\|$ after $t = 5$ s, and also strong correlations of $\|\boldsymbol{\varepsilon}_{ndi}\|$ with the fault degree. As a consequence, the $\boldsymbol{K}_s$ used in NDI-SMC/SMDO must be adapted or manually adjusted in different scenarios. For the simulation cases shown in Fig. 6, $\boldsymbol{K}_s = \text{diag}([4, 5, 3, 8])$ is used when no actuator fault occurs. To guarantee the convergence of $\boldsymbol{s}$, $\boldsymbol{K}_s$ needs to be increased to $\text{diag}([50, 40, 4, 10])$ for the '25% fault' case, and be further raised to $\text{diag}([150, 90, 5, 12])$ when half of the rotor effectiveness is lost. These gain increases induce a side effect, chattering. As illustrated by Fig. 6, the oscillation magnitudes of $\hat{\boldsymbol{v}}_{eq}$ increase with the rise of $\boldsymbol{K}_s$.

Furthermore, in view of Eq. (10), an increase of $\boldsymbol{K}_s$ will lead to the oscillations in the control input. It can be seen from Fig. 7 that even though filtered by the actuator dynamics, the measured (without noise in simulations) rotor speeds are still oscillating. In addition, ω_3 in Fig. 7 increases after $t = 5$ s to compensate for the effectiveness loss.
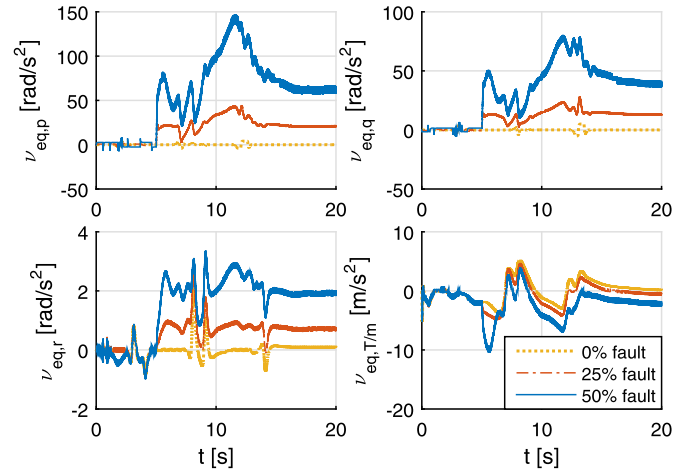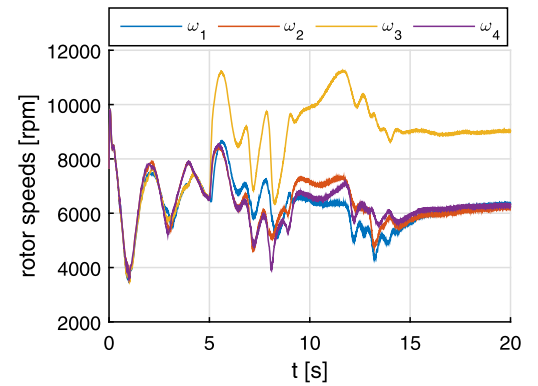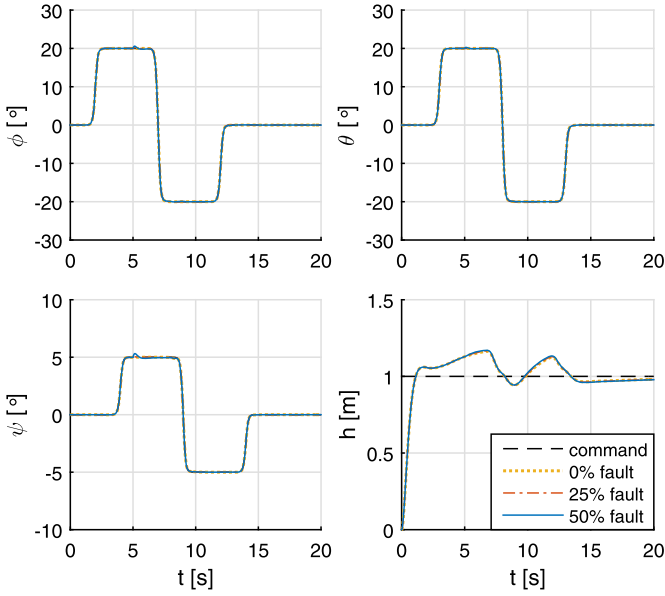
Fig. 8. Quadrotor responses under INDI-SMC/SMDO control.
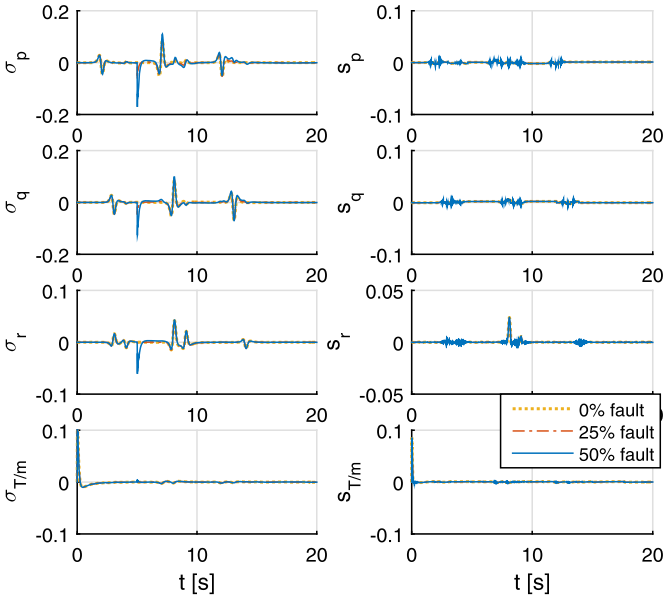
Fig. 9. Responses of sliding variables under INDI-SMC/SMDO control.

Fig. 10. Observed uncertainties $\hat{\boldsymbol{v}}_{\mathrm{eq}}$ under INDI-SMC/SMDO control.
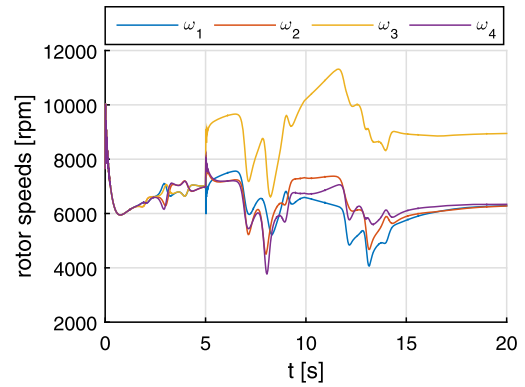
Fig. 11. Measured rotor speeds under INDI-SMC/SMDO control in the '50% fault' case.

curs, the term $\boldsymbol{\delta}_d + (\boldsymbol{G}_f - \bar{\boldsymbol{G}})\Delta \boldsymbol{u}_{\mathrm{indi}}$ is added to $\boldsymbol{\varepsilon}_{\mathrm{indi}}$, which also has smaller changes in different fault cases as verified by Fig. 10.

These beneficial properties of $\boldsymbol{\varepsilon}_{\mathrm{indi}}$ allow a lower and fixed gain matrix $\boldsymbol{K}_s = \mathrm{diag}([2, 2, 0.5, 1])$ to be used for resisting all the tested perturbations, which simplifies the implementation process, and fundamentally reduces the chattering effects of SMC/SMDO. As can be seen by comparing Fig. 10 with Fig. 6, the uncertainty observations $\hat{\boldsymbol{v}}_{\mathrm{eq}}$ are much smoother when using INDI-SMC/SMDO. The rotor speeds in Fig. 11 are also much smoother than those shown in Fig. 7.

5. Experimental validations

5.1. Experimental setup

The performance and robustness of the proposed INDI-SMC/SMDO controller are further validated via flight tests. These experiments are conducted using a Parrot Bebop 2 quadrotor as shown
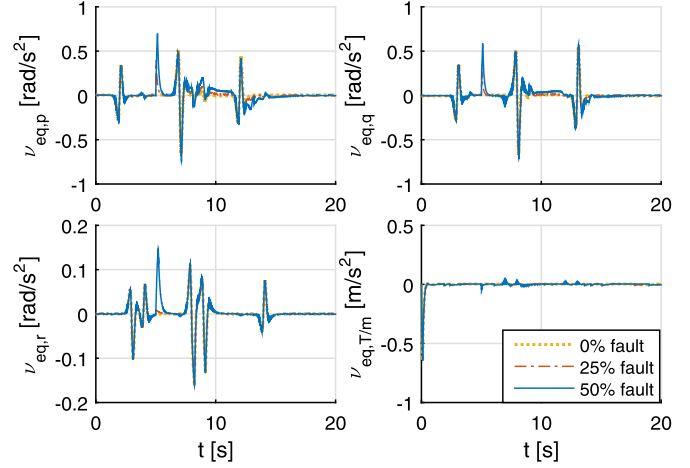
in Fig. 12. The control laws are executed on-board using an open-source autopilot software, Paparazzi, which is able to read the MPU 6050 Inertia Measurement Unit (IMU) measurements and drive the motors at 512 Hz. The position and attitude are measured by external motion capture system (OptiTrack) in 120 Hz and transmitted to the on-board controller via Wi-Fi.

Some practical issues should be considered before implementing the INDI-SMC/SMDO control law. The first issue is the way of obtaining $\dot{\boldsymbol{\Omega}}_0$ when applying Eqs. (19, 36) in the inner-loop. The feasibility of directly measuring $\dot{\boldsymbol{\Omega}}_0$ via angular accelerometers has been demonstrated in Ref. [43]. Another simple way is estimating $\dot{\boldsymbol{\Omega}}_0$ from gyroscope measurements using a wash-out filter [26]. To deal with the corresponding lag, the input signal should be synchronized with the estimations. Since this way of estimation and synchronization has been verified via both passenger aircraft and quadrotor flight tests [26,27,23], it is also adopted in the present flight tests. T_0/m in Eq. (36) is calculated from the specific force measured by linear accelerometers. The rotor speed $\boldsymbol{u}_{\mathrm{indi}}|_0$ is measured by the Brushless DC Motor Driver of the Bebop2 quadrotor.

The outer-loop controllers used in flight tests are identical with the simulated controllers. For the inner-loop, $\boldsymbol{K}_\sigma$ is still equal to $\mathrm{diag}([0.5, 0.5, 0.5, 1])$, while $\boldsymbol{\tau}$ is increased to $[0.1, 0.1, 0.17, 0.1]^T$ for attenuating the measurement noise. An estimated constant control effectiveness matrix $\bar{\boldsymbol{G}}$ is used by both NDI and INDI based controllers. The nominal model $\bar{\boldsymbol{f}}$ used by NDI-SMC/SMDO is a hover model which excludes aerodynamic effects, gyroscopic moments and spin-up torque. As shown in Eqs. (13, 19), INDI-SMC/SMDO does not need the model information $\bar{\boldsymbol{f}}$.

Both controllers are tested in two scenarios: with and without actuator faults. Even if four unbroken rotors are equipped, model

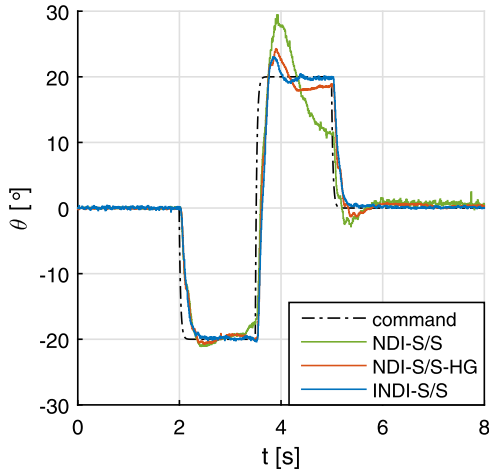Fig. 12. A Bebop 2 quadrotor with one damaged rotor.

Fig. 13. Quadrotor tracking responses without actuator fault. (For interpretation of the colors in the figure(s), the reader is referred to the web version of this article.)

Fig. 14. Observed uncertainties $\hat{\boldsymbol{\nu}}_{eq}$ without actuator fault.

Fig. 15. Sliding variable responses without actuator fault.

mismatches still exist, which become more conspicuous when airspeed increases during maneuvers. For the faulty configuration, the diameter of the right rear rotor disk (third) is reduced by 5 cm as shown by Fig. 12, which approximately reduce its effectiveness by 55% according to flight test results.

5.2. Flights without actuator fault

The SMDO gain matrix $\boldsymbol{K}_s = \mathrm{diag}([20, 20, 1, 1])$ is used by INDI-SMD/SMDO in flight tests. The $\boldsymbol{K}_s$ used by NDI-SMC/SMDO is first tuned to be identical to the INDI based, as denoted by 'NDI-S/S' in the subsequent figures, then it is increased to ensure the convergence of s as denoted by 'NDI-S/S-HG'.

Fig. 13 illustrates the responses of a quadrotor tracking a filtered doublet pitch angle command. When using INDI-SMC/SMDO control, the quadrotor performs the best with smallest overshoots and tracking errors. Although NDI based SMC/SMDO control using the same $\boldsymbol{K}_s$ is able to follow the command, large transition errors are present. This performance deterioration is mainly caused by model uncertainties. As also shown by Fig. 14, 'NDI-S/S', which uses the same $\boldsymbol{K}_s$ as 'INDI-S/S', is unable to adequately observe the uncertainties in pitch, yaw and thrust channels. The large variations of $\boldsymbol{\varepsilon}_{ndi}$ can only be observed when $\boldsymbol{K}_s$ is raised to $\mathrm{diag}([20, 50, 20, 10])$, as shown by the high-gain 'NDI-S/S-HG' in Fig. 14. This high-gain controller performs better than the low-gain 'NDI-S/S', but is still inferior than INDI based SMC/SMDO as illustrated by Fig. 13.

It can also be seen from Fig. 14 that the observed uncertainties under INDI based control have smaller variations. Increasing the switching gains in NDI-SMC/SMDO can better observe $\boldsymbol{\varepsilon}_{ndi}$, but
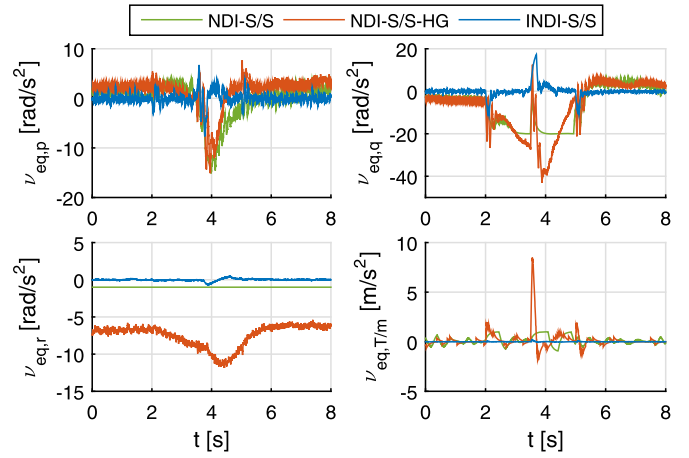
consequently cause severe oscillations, especially in pitch and yaw channels.

The responses of the sliding variables are presented in Fig. 15. As is consistent with the above analyses, using the same $\boldsymbol{K}_s$ with INDI based control is insufficient for NDI-SMC/SMDO, because s_r diverges, and s_q, s_T are absent from the sliding surfaces for about two seconds. Moreover, σ_r under low-gain NDI based control also diverges. High-gain NDI-SMC/SMDO can enforce the convergence of $\boldsymbol{\sigma}$ and s. However, severe oscillations in s_q are present, and the convergence of σ_q, $\sigma_{T/m}$ is still slower than the response under INDI-SMC/SMDO control.

5.3. Flights with actuator fault

This subsection presents the flight test results of NDI and INDI based SMC/SMDO controllers applied to a quadrotor with one damaged rotor (Fig. 12). As verified by simulations, INDI based SMC/SMDO is able to passively tolerate actuator faults and model uncertainties, thus the same SMDO gain matrix $\boldsymbol{K}_s = \mathrm{diag}([20, 20, 1, 1])$ is still used by the faulty quadrotor. However, this gain matrix is insufficient for NDI based SMC/SMDO, even without actuator fault, as shown in the previous subsection. There-
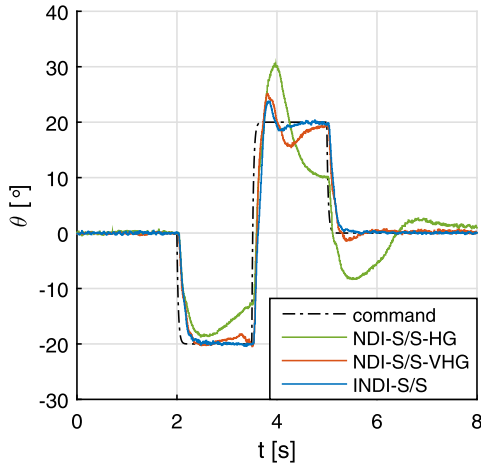
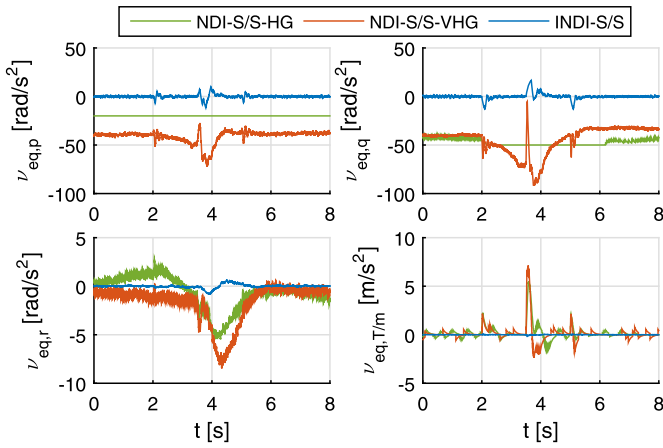**Fig. 16.** Quadrotor tracking responses with actuator fault.

Fig. 17. Observed uncertainties $\hat{\nu}_{eq}$ with actuator fault.
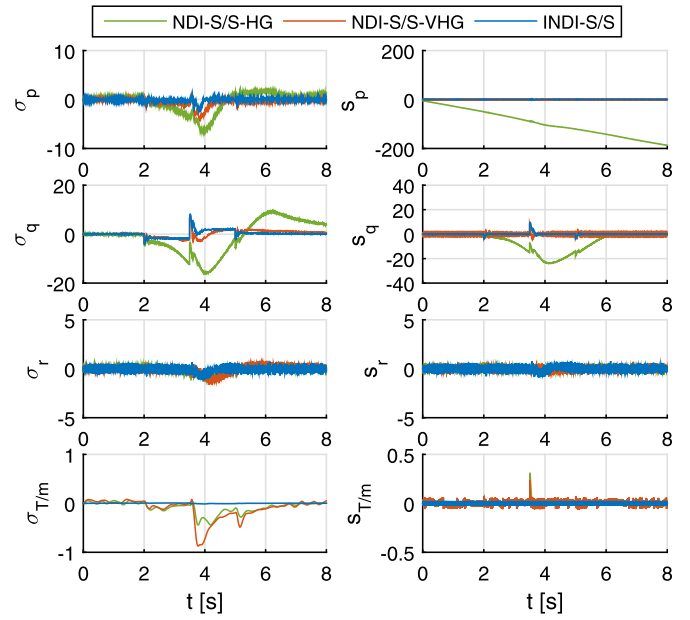

Fig. 18. Sliding variable responses with actuator fault.

Fig. 19. Rotor speeds using NDI (left) and INDI (right) based SMC/SMDO in faulty condition.

fore, in this subsection, it is going to be tested whether NDI based SMC/SMDO can passively resist the actuator fault without gain adjustment. Namely, $K_s = \text{diag}([20, 50, 20, 10])$ is used by NDI based controller first, as denoted by 'NDI-S/S-HG' in the subsequent figures.

Fig. 16 shows that although the faulty quadrotor can follow the trend of command without gain adjustment, its performance deteriorates. Recall from Eq. (7) that actuator faults introduce $(f_f - \bar{f}) + (G_f - \bar{G})u_{ndi}$ into ε_{ndi}. This term causes large variations in $\|\varepsilon_{ndi}\|$ after fault occurs because u_{ndi} is far from zero for trimming the quadrotor. Therefore, as exposed by Fig. 17, the gain matrix tuned for the fault-free case is insufficient, which leads to saturations in the observed uncertainties in the pitch and roll channels. In order to fully observe the uncertainties, K_s needs to be increased to $\text{diag}([80, 100, 20, 10])$ according to the flight test results. This very high gain control case is denoted by 'NDI-S/S-VHG' in Fig. 16–19. This controller with even higher switching gains can better observe $-\varepsilon_{ndi}$ as shown in Fig. 17, and consequently improve the tracking performance as illustrated in Fig. 16.

On the contrary, INDI-SMC/SMDO is able to tolerate the actuator fault passively *without any* gain adjustment. In view of Fig. 17, the observed $-\varepsilon_{indi}$ has much smaller oscillations as compared to the observed $-\varepsilon_{ndi}$. Moreover, as shown in Fig. 16, INDI-SMC/SMDO performs the best with smallest transition errors. Analogous to the above analyses, when using NDI-SMC/SMDO control without gain adjustment, s_p diverges and s_q is absence from the sliding surface throughout the maneuvering time period, as illustrated by Fig. 18. Even though without gain adaption, the sliding variables σ and s under INDI-SMC/SMDO control have the highest convergence rates and lightest oscillations among all the tested controllers.

Reducing the switching gains is crucial for chattering reduction of SMC/SMDO methods. As verified by both simulations and flight tests, the filtering process in SMDO can only attenuate instead of rejecting the oscillations in $\hat{\nu}_{eq}$. Therefore, the lower gains used by INDI-SMC/SMDO also lead to lighter oscillations in $\hat{\nu}_{eq}$ (Fig. 10, 14, 17) and in the rotor speeds (Fig. 11).

The rotor speeds under the control of very-high-gain NDI-SMC/SMDO and INDI-SMC/SMDO are shown in Fig. 19. The first rotor get saturated at 3000 rpm for 0.3 s under NDI-SMC/SMDO control, while the rotor speeds are within limits using INDI-SMC/SMDO. Owing to the measurement noise, the chattering reduction advantage of INDI based SMC/SMDO becomes less obvious in Fig. 19, where the rotor speeds using NDI and INDI based controllers seem to have comparable oscillations.

The reason behind this phenomenon can be better revealed in the frequency domain. Divide u_{ndi} (Eq. (10)) into $u_{ndi,s} = \bar{G}^{-1}(K_\sigma \sigma + \hat{\nu}_{eq})$ (the contributions of SMC/SMDO), and $u_{ndi,c} = \bar{G}^{-1}\bar{\Psi}$ (the contributions of the traditional NDI). Also, u_{indi} (Eq. (19)) is divided into $u_{indi,s} = \bar{G}^{-1}(K'_\sigma \sigma + \hat{\nu}'_{eq})$ and $u_{indi,c} =$
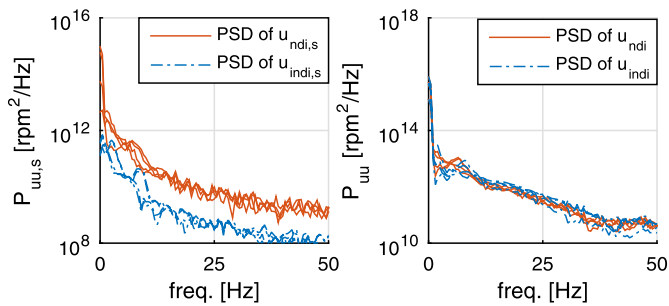
Fig. 20. The left subplot presents the PSD of $\boldsymbol{u}_{\mathrm{ndi},s}$, $\boldsymbol{u}_{\mathrm{indi},s}$, while the right shows the PSD of $\boldsymbol{u}_{\mathrm{ndi}}$, $\boldsymbol{u}_{\mathrm{indi}}$.

$\boldsymbol{u}_{\mathrm{indi}}|_0 + \bar{\boldsymbol{G}}^{-1}\bar{\boldsymbol{\Psi}}'$. The Power Spectral Densities (PSD) of u_{ndi,s_i} and u_{indi,s_i}, $i = 1, 2, 3, 4$ for the four rotors are illustrated in the left subplot of Fig. 20, where it can be seen that $P_{\boldsymbol{uu},\mathrm{indi},s}$ is lower than $P_{\boldsymbol{uu},\mathrm{ndi},s}$ in most frequency ranges. This verifies that the control efforts of SMC/SMDO is indeed released using the INDI control structure, and the chattering is reduced in $\boldsymbol{u}_{\mathrm{indi},s}$. On the other hand, INDI-SMC/SMDO is contributed more by $\boldsymbol{u}_{\mathrm{indi},c}$, which has less model dependency than $\boldsymbol{u}_{\mathrm{ndi},c}$ but relies more on sensor measurements. The corresponding measurement noise in $\boldsymbol{u}_{\mathrm{indi},c}$ conceals the benefit of $\boldsymbol{u}_{\mathrm{indi},s}$ in high frequency range, and leads to a comparable PSD of the overall $\boldsymbol{u}_{\mathrm{indi}}$ and $\boldsymbol{u}_{\mathrm{ndi}}$ as illustrated by the right subplot of Fig. 20. The noise level in $\boldsymbol{u}_{\mathrm{indi},c}$ can be reduced by using better sensors, which can be easier than perfecting the model used by NDI-SMC/SMDO.

6. Conclusions

A control method named INDI-SMC/SMDO, which designs the Sliding Mode Control (SMC) driven by Sliding Mode Disturbance Observers (SMDO) based on the control structure of Incremental Nonlinear Dynamics Inversion (INDI) is proposed in this paper. By virtue of the sensor-based characteristic of INDI, SMC/SMDO designs based on INDI require less model knowledge than designs based on NDI. In the presence of model uncertainties, external disturbances and sudden faults, it has been shown both analytically and numerically that the perturbation terms under NDI and INDI based SMC/SMDO control ($\boldsymbol{\varepsilon}_{\mathrm{ndi}}$ and $\boldsymbol{\varepsilon}_{\mathrm{indi}}$) have different properties. First of all, the boundedness of $\boldsymbol{\varepsilon}_{\mathrm{indi}}$ is guaranteed when the conditions in Theorem 2 are satisfied, while the boundedness of $\boldsymbol{\varepsilon}_{\mathrm{ndi}}$ is undetermined under the same conditions. More importantly, there exists a sampling frequency that makes the upper bound of $\boldsymbol{\varepsilon}_{\mathrm{indi}}$ is smaller than that of $\boldsymbol{\varepsilon}_{\mathrm{ndi}}$, which can fundamentally reduce the control efforts of SMC/SMDO because for most SMC and SMDO designs, there is a positive correlation between the required switching gains and the uncertainty bounds. $\boldsymbol{\varepsilon}_{\mathrm{indi}}$ is also proved to have smaller variations in different fault circumstances, while $\boldsymbol{\varepsilon}_{\mathrm{ndi}}$ is more fault-case dependent. These merits of $\boldsymbol{\varepsilon}_{\mathrm{indi}}$ allow INDI-SMC/SMDO to use reduced and fixed gains for resisting a wider variety of faults and disturbances, while the gains for NDI based SMC/SMDO are higher and require adjustments in different scenarios. Finally, the advantages of INDI-SMC/SMDO are demonstrated by both numerical simulations and real-world quadrotor flight tests. In conclusion, easier implementation, reduced model dependency, improved performance and robustness make the proposed INDI-SMC/SMDO a promising method for enhancing aircraft safety in real life.

Conflict of interest statement

There is no conflict of interest.

References

[1] J.K. Stolaroff, C. Samaras, E.R. O'Neill, A. Lubers, A.S. Mitchell, D. Ceperley, Energy use and life cycle greenhouse gas emissions of drones for commercial package delivery, Nat. Commun. 9 (2018) 409.

[2] J.-J.E. Slotine, W. Li, Applied Nonlinear Control, Prentice Hall, Englewood Cliffs, NJ, 1991.

[3] J.Y. Hung, W. Gao, J.C. Hung, Variable structure control: a survey, IEEE Trans. Ind. Electron. 40 (1993) 2–22.

[4] R. Xu, U. Ozguner, Sliding mode control of a quadrotor helicopter, in: Proceedings of the 45th IEEE Conference on Decision and Control, 2006, pp. 4957–4962.

[5] D. Lee, H.J. Kim, S. Sastry, Feedback linearization vs. adaptive sliding mode control for a quadrotor helicopter, Int. J. Control. Autom. Syst. 7 (2009) 419–428.

[6] F. Sharifi, M. Mirzaei, B.W. Gordon, Y. Zhang, Fault tolerant control of a quadrotor UAV using sliding mode control, in: 2010 Conference on Control and Fault-Tolerant Systems (SysTol), 2010, pp. 239–244.

[7] T. Li, Y. Zhang, B.W. Gordon, Passive and active nonlinear fault-tolerant control of a quadrotor unmanned aerial vehicle based on the sliding mode control technique, in: Special Issue Article Proc IMechE Part I, Syst. Sci. Control Eng. 227 (2012) 12–23.

[8] L. Besnard, Y.B. Shtessel, B. Landrum, Quadrotor vehicle control via sliding mode controller driven by sliding mode disturbance observer, J. Franklin Inst. 349 (2012) 658–684.

[9] A.R. Merheb, H. Noura, F. Bateman, Design of passive fault-tolerant controllers of a quadrotor based on sliding mode theory, Int. J. Appl. Math. Comput. Sci. 25 (2015) 561–576.

[10] A. Modirrousta, M. Khodabandeh, A novel nonlinear hybrid controller design for an uncertain quadrotor with disturbances, Aerosp. Sci. Technol. 45 (2015) 294–308.

[11] S. Rajappa, C. Masone, H.H. Bulthoff, P. Stegagno, Adaptive Super Twisting Controller for a quadrotor UAV, in: Proceedings - IEEE International Conference on Robotics and Automation 2016-June, 2016, pp. 2971–2977.

[12] Y. Yang, Y. Yan, Attitude regulation for unmanned quadrotors using adaptive fuzzy gain-scheduling sliding mode control, Aerosp. Sci. Technol. 54 (2016) 208–217.

[13] F. Mu, M. Bonilla, E.S. Espinoza, Robust trajectory tracking for unmanned aircraft systems using high order sliding mode controllers-observers, in: 2017 International Conference on Unmanned Aircraft Systems (ICUAS), Miami, Florida, 2017.

[14] Z. Jia, J. Yu, Y. Mei, Y. Chen, Y. Shen, X. Ai, Integral backstepping sliding mode control for quadrotor helicopter under external uncertain disturbances, Aerosp. Sci. Technol. 68 (2017) 299–307.

[15] V.I. Utkin, A.S. Poznyak, Adaptive sliding mode control with application to super-twist algorithm: equivalent control method, Automatica 49 (2013) 39–47.

[16] C. Edwards, Y.B. Shtessel, Continuous higher order sliding mode control based on adaptive disturbance compensation, in: 2014 13th International Workshop on Variable Structure Systems (VSS), vol. 47, IEEE, 2014, pp. 1–5.

[17] C. Edwards, Y. Shtessel, Adaptive dual-layer super-twisting control and observation, Int. J. Control 89 (2016) 1759–1766.

[18] C. Edwards, Y.B. Shtessel, Adaptive continuous higher order sliding mode control, Automatica 65 (2016) 183–190.

[19] C.E. Hall, Y.B. Shtessel, Sliding mode disturbance observer-based control for a reusable launch vehicle, J. Guid. Control Dyn. 29 (2006) 1315–1328.

[20] P.M. Tiwari, S. Janardhanan, M. Un Nabi, Attitude control using higher order sliding mode, Aerosp. Sci. Technol. 54 (2016) 108–113.

[21] M. Defoort, T. Floquet, A. Kokosy, W. Perruquetti, A novel higher order sliding mode control scheme, Syst. Control Lett. 58 (2009) 102–108.

[22] T.E. Massey, Y.B. Shtessel, Continuous traditional and high-order sliding modes for satellite formation control, J. Guid. Control Dyn. 28 (2005) 826–831.

[23] F. Grondman, G. Looye, R.O. Kuchar, Q.P. Chu, E. Van Kampen, Design and flight testing of incremental nonlinear dynamic inversion-based control laws for a passenger aircraft, in: 2018 AIAA Guidance, Navigation, and Control Conference, January, AIAA, Kissimmee, Florida, 2018.

[24] X. Wang, E. Van Kampen, Q.P. Chu, P. Lu, Stability analysis for incremental nonlinear dynamic inversion control, J. Guid. Control Dyn. (2019), published online, https://arc.aiaa.org/doi/10.2514/1.G003791.

[25] S. Sieberling, Q.P. Chu, J.A. Mulder, Robust flight control using incremental nonlinear dynamic inversion and angular acceleration prediction, J. Guid. Control Dyn. 33 (2010) 1732–1742.

[26] E.J.J. Smeur, Q.P. Chu, G.C.H.E. de Croon, Adaptive incremental nonlinear dynamic inversion for attitude control of micro air vehicles, J. Guid. Control Dyn. 39 (2016) 450–461.

[27] E.J. Smeur, G.C. de Croon, Q. Chu, Gust disturbance alleviation with Incremental Nonlinear Dynamic Inversion, in: 2016 IEEE/RSJ International Conference on Intelligent Robots and Systems (IROS), IEEE, 2016, pp. 5626–5631.

[28] X. Wang, E. van Kampen, Q. Chu, P. Lu, Incremental sliding-mode fault-tolerant flight control, J. Guid. Control Dyn. 42 (2019) 244–259.

[29] S. Sun, L. Sijbers, X. Wang, C. de Visser, High-speed flight of quadrotor despite loss of single rotor, IEEE Robot. Autom. Lett. 3 (2018) 3201–3207.

[30] Y.B. Shtessel, J.M. Buffington, S.S. Banda, Multiple timescale flight control using reconfigurable sliding modes, J. Guid. Control Dyn. 22 (1999) 873–883.

[31] Y. Shtessel, J. Buffington, S. Banda, Tailless aircraft flight control using multiple time scale reconfigurable sliding modes, IEEE Trans. Control Syst. Technol. 10 (2002) 288–296.

[32] Y.B. Shtessel, I.A. Shkolnikov, Aeronautical and space vehicle control in dynamic sliding manifolds, Int. J. Control 76 (2003) 1000–1017.

[33] V. Utkin, J. Shi, Integral sliding mode in systems operating under uncertainty conditions, in: Proceedings of 35th IEEE Conference on Decision and Control, vol. 4, 1996, pp. 1–6.

[34] H.K. Khalil, Nonlinear Systems, pdf, Prentice-Hall, New Jersey, 2002.

[35] P. Acquatella, E. van Kampen, Q.P. Chu, Incremental backstepping for robust nonlinear flight control, in: CEAS Conference on Guidance, Navigation, and Control, 2013, pp. 1444–1463.

[36] X. Wang, E.-J. Van Kampen, Incremental backstepping sliding mode fault-tolerant flight control, in: AIAA Scitech 2019 Forum, 2019, pp. 1–23.

[37] X. Shao, Q. Meng, J. Liu, H. Wang, RISE and disturbance compensation based trajectory tracking control for a quadrotor UAV without velocity measurements, Aerosp. Sci. Technol. 74 (2018) 145–159.

[38] X. Shao, J. Liu, H. Cao, C. Shen, H. Wang, Robust dynamic surface trajectory tracking control for a quadrotor UAV via extended state observer, Int. J. Robust Nonlinear Control 28 (2018) 2700–2719.

[39] Y. Song, L. He, D. Zhang, J. Qian, J. Fu, Neuroadaptive fault-tolerant control of quadrotor UAVs: a more affordable solution, IEEE Trans. Neural Netw. Learn. Syst. (2018) 1–9.

[40] B. Etkin, Dynamics of Atmospheric Flight, Dover Publications, Toronto, 2005.

[41] S. Sun, R. Schilder, C.C. de Visser, Identification of quadrotor aerodynamic model from high speed flight data, in: 2018 AIAA Atmospheric Flight Mechanics Conference, January, American Institute of Aeronautics and Astronautics, Kissimmee, Florida, 2018, pp. 1–23.

[42] X. Wang, E. Van Kampen, Q.P. Chu, Gust load alleviation and ride quality improvement with incremental nonlinear dynamic inversion, in: AIAA Atmospheric Flight Mechanics Conference, American Institute of Aeronautics and Astronautics, Grapevine, Texas, 2017, pp. 1–21.

[43] T. Keijzer, G. Looye, Q.P. Chu, E. Van Kampen, Design and flight testing of incremental backstepping based control laws with angular accelerometer feedback, in: 2019 AIAA Guidance, Navigation, and Control Conference, January, AIAA, San Diego, California, 2019.